Wide-Band CDMA for the UMTS/IMT-2000 Satellite Component

Daniel Boudreau, Giuseppe Caire, *Member, IEEE*, Giovanni Emanuele Corazza, *Member, IEEE*, Riccardo De Gaudenzi, *Senior IEEE*, Gennaro Gallinaro, Michele Luglio, R. Lyons, Javier Romero-García, A. Vernucci, and Hanspeter Widmer

***Abstract*—This paper describes the main aspects relevant to the development of a third-generation radio transmission technology (RTT) concept identified as satellite wide-band CDMA (SW-CDMA), which has been accepted [1] by the International Telecommunications Union (ITU) as one of the possible RTTs for the satellite component of International Mobile Telecommunications-2000 (IMT-2000). The main outcomes of the extensive system engineering effort that has led to the above ITU RTT are described. In particular, we address propagation channel characteristics, satellite diversity, power control, pilot channel, code acquisition, digital modulation and spreading format, interference mitigation, and resource allocation. Due to its similarity with respect to the terrestrial W-CDMA proposal from which it is derived, the SW-CDMA *open* air interface solution is described briefly, with emphasis only on the major adaptation required to best cope with the satellite environment. Quantitative results concerning the physical-layer performance over realistic channel conditions, for both forward and reverse link, are reported. A system capacity study case for a low-earth-orbit constellation is also provided.**

***Index Terms*—Code division multiaccess, fading channels, power control, satellite mobile, source coding.**

Manuscript received April 17, 2000; revised July 27, 2001. This work was supported by the European Space Agency under Contract number 12497/97/NL/NB

D. Boudreau was with Communications Research Centre, Ottawa, ON K2H 8S2, Canada. He is now with Nortel Networks, Brampton, ON L6T 5P6, Canada (danielbo@nortelnetworks.com).

G. Caire was with the Politecnico di Torino, I-10129 Torino, Italy. He is now with Mobile Communications Group, Institut EURECOM, B. P. 193 06904 Sophia Antipolis Cedex, France (e-mail: caire@eurecom.fr).

G. E. Corazza was with the Department of Electronic Engineering, University of Rome "Tor Vergata," 00133 Rome, Italy. He is now with DEIS, the University of Bologna, 40137 Bologna, Italy.

R. De Gaudenzi is with ESA-ESTEC (TOS-ETC), 2200 AG Noordwijk, The Netherlands (e-mail: rdegaude@estec.esa.nl).

G. Gallinaro and A. Vernucci are with Space Engineering S.p.A., I-00155 Rome, Italy (e-mail: gallinaro@space.it; vernucci@space.it).

M. Luglio is with the Dipartimento di Ingegneria Elettronica, University of Roma "Tor Vergata," 00133 Rome, Italy (e-mail: Michele.Luglio@uniroma2.it).

R. Lyons is with Square Peg Communications, Inc., Kanata, ON K2K 2A3, Canada (e-mail: rlyonss@mail.magma.ca).

J. Romero-García was with the Eurpoean Space Agency, 75738 Paris, France. He is now with Nokia RAS/SDA/Wireless Network Performance Málaga System Competence Center, Málaga, Spain (e-mail: Javier.Romero@nokia.com).

H. Widmer is with the Ascom Systec AG, Technology Unit, CH-5506 Maegenwil, Switzerland (e-mail: hanspeter.widmer@ascom.ch).

Publisher Item Identifier S 0018-9545(02)00426-7.

NOMENCLATURE

AFC	Automatic frequency control.
AWGN	Additive white Gaussian noise.
BER	Bit error rate.
BP	Burst pilot.
BPSK	Binary phase-shift keying.
CCPCH	Common control physical channel.
CDM	Code-division multiplexing.
CDMP	Code-division multiplexed pilot.
C/M	Carrier-over-multipath ratio.
CPAFC	Cross-product automatic frequency control.
CR	Correlation receiver.
CRC	Cyclic redundancy check.
CW	Continuous wave.
DA	Data-aided.
DD	Decision-directed.
DLL	Delay-locked loop.
DPCCH	Dedicated physical control channel.
DPDCH	Dedicated physical data channel.
EC-BAID	Extended complex blind adaptive interference detector.
ETSI	European Telecommunication Standardization Institute.
FDMA	Frequency-division multiple access.
FEC	Forward error correction.
FER	Frame error rate.
FF	Fast fading.
FFT	Fast Fourier transform.
FL	Forward link.
GEO	Geostationary earth orbiting satellite.
HPA	High-power amplifier.
HW	Hardware.
IMT-2000	International Mobile Telecommunication-2000.
ITU	International Telecommunication Union.
LEO	Low earth orbiting satellite.
LMMSE	Linear minimum mean square error.
LMS	Least mean square.
LOS	Line of sight.
MAI	Multiple access interference.
MEO	Medium earth orbiting satellite.
MES	Mobile earth station.
MOE	Minimum output energy.
MUD	Multiuser detector.
NDA	Non-data-aided.
O-CDMA	Orthogonal code-division multiple access.
OVSF	Orthogonal variable spreading sequence factor.

PCC	Power control command.
PDSCH	Physical downlink shared channel.
PRACH	Physical random-access channel.
PSD	Power spectral density.
QPSK	Quadrature phase-shift keying.
RACH	Random-access channel.
RL	Reverse link.
RLS	Recursive least square.
RP	Relative power.
RTT	Radio transmission technique.
SCH	Synchronization channel.
SF	Slow fading.
SNIR	Signal-to-noise plus interference ratio.
SNR	Signal-to-noise ratio.
SSPA	Solid-state power amplifier.
S-UMTS	Satellite Universal Mobile Telecommunication System.
SUMF	Single-user matched filter.
SW-CDMA	Satellite wide-band code-division multiple access.
SW-CTDMA	Satellite wide-band code- and time-division multiple access.
TC	Threshold crossing.
TD-CDMA	Time-division code-division multiple access.
TDMA	Time-division multiple access.
TDMP	Time-division multiplexed pilot.
TFCI	Transport format control information.
TPC	Transmit power control.
UMTS	Universal Mobile Telecommunication System.
W-CDMA	Wideband code-division multiple access.

I. Introduction

IN THE general IMT-2000 standardization framework promoted by the ITU, the UMTS sponsored by ETSI aims at the definition of a unified third-generation global wireless system operating in the 2-GHz band. UMTS is expected to support a wide range of connection-oriented and connectionless services with data rates up to 384 kbit/s in outdoor environments and up to 2 Mbit/s in indoor environments. The service bit rate can be negotiated at call setup and flexibly modified on a frame-by-frame basis. Through service and terminal class definition, the standardization effort has identified the core network functionalities that are independent of air interface. While the radio-independent core network will most likely encompass heterogeneous network technologies, radio technologies are being standardized in order to maximize the global system nature. A large effort recently has been completed for the selection of a few RTT proposals capable of efficiently supporting the IMT-2000 requirements by means of both terrestrial and satellite networks.

The global IMT-2000 nature calls for service provision in a host of environments ranging from indoor picocells to satellite macrocells. The fundamental satellite role in providing coverage over scarcely populated regions for true global roaming or for efficient multicasting service provision has been widely recognized in UMTS. For the first time, the satellite is seen as an integral part of a cellular global communication network, although due to technological and physical constraints, satellite services can only represent a subset of those provided by terrestrial UMTS. Successful satellite integration within UMTS calls for the definition of an efficient, yet flexible, RTT well matched to the satellite mobile environment.

In this framework, ESA has undertaken studies on S-UMTS heading to the now-approved RTT proposal, the main results of which are summarized in this paper. The S-UMTS RTT definition has been performed with particular attention to the ongoing T-UMTS standardization activities performed in the Third-Generation Partnership Program (3GPP) [17] in order to maximize commonality. Current evolutions of terrestrial standards are closely followed and will be integrated in the S-UMTS shortly after. Use of common S/T-UMTS technologies will in fact contribute to largely reducing dual-mode user terminals' cost and size, thus boosting S-UMTS commercial opportunities. The cost/size reduction will be eased by the fact that T-UMTS and S-UMTS are allocated adjacent frequency bands.

As is known, the 3GPP T-UMTS proposal encompasses two operating modes: W-CDMA, associated with frequency-division duplex, and TD-CDMA, associated with time-division duplex. We considered both operating modes and adapted them to the satellite environment, which resulted in the two proposals identified as SW-CDMA and SW-CTDMA [1]. This paper focuses only on SW-CDMA for its more general applicability. As far as SW-CTDMA is concerned, suffice it to say that it may be a suitable solution for regional systems adopting geostationary or elliptical orbits when the terminal peak effective isotropic radiated power (EIRP) can be relatively large. More details can be found in [1].

Commonality with T-UMTS is not the only reason for adopting CDMA in S-UMTS. As reported in [2] and [3], the main drivers for CDMA selection are:

1) higher capacity than TDMA in most situations;
2) universal frequency reuse, easing resource allocation;
3) capability of soft satellite beam handoff;
4) exploitation of satellite diversity for improved quality of service and fading effects mitigation
5) mobile terminal (MT) moderate EIRP requirements;
6) applicability of interference mitigation techniques;
7) flexible support of a wide range of services;
8) provision of accurate user positioning;
9) graceful degradation under loaded condition;
10) simplified satellite antenna design [16];
11) compatibility with adaptive antennas.

Finally, the low power spectral density nature of spread-spectrum signals certainly helps in satisfying the respective regulatory constraints.

The SW-CDMA proposal has been devised independently from a specific satellite orbital configuration in order to represent as much as possible a flexible standard. However, with the focus on global systems, the adoption of LEO or MEO satellite constellations seems most appropriate, as they can be designed to allow almost global coverage of densely populated regions with large probability of multiple satellite visibility. GEO constellations can also represent more attractive solutions from the business point of view for the lower investments required. Also,

from the acquisition and channel estimation point of view, LEO orbits are the most demanding, and they can be considered as a benchmark. Therefore, the following discussion will assume the adoption of a LEO constellation, although the SW-CDMA RTT can be adopted for MEO/GEO-based system architectures as well.

This paper is organized as follows. In Section II, we report on the main system engineering considerations and tradeoffs that have led to the SW-CDMA proposal. This is a somewhat unusual section in that motivations behind standards choices are usually not reported in the open literature. The proposed SW-CDMA *open* air interface solution is described in some detail in Section III. Due to its similarity with respect to the terrestrial W-CDMA proposal, emphasis is placed only on the main characteristics and major differences, as for example the fact that we allow for the use of interference mitigation techniques on the mobile terminal. This is due to the fact that system capacity for the LEO system exploiting path diversity appears to be limited by the FL and not by the RL. In a single GEO case, the system is typically reverse-link capacity limited. However, it is expected that the majority of multimedia services will require a larger forward-link throughput. Quantitative results concerning the physical-layer performance over realistic channel conditions, for both FL and RL, are reported in Section IV, where end-to-end performance including source coding for speech and video services is also considered, although not directly related to the RTT. Section V provides the system capacity results for a LEO constellation study case. Conclusions are drawn in Section VI.

II. System Engineering for SW-CDMA

In this section, we report the main system engineering considerations, tradeoff, and analyses that have led to the proposal submitted to ITU. In particular, we address propagation channel characteristics, satellite diversity, power control, pilot channel insertion, code acquisition, modulation and spreading format, interference mitigation, and resource allocation.

A. Propagation Channel Characteristics

As for any wireless system, channel characteristics should play a key role in the definition of an S-UMTS RTT. Note that propagation conditions are quite different for LEO/MEO S-UMTS with respect to T-UMTS. In fact, the T-UMTS channel is typically affected by log-normal long-term shadowing and Rayleigh short-term multipath fading, with generally no LOS component, except possibly in picocellular environments. In these conditions, the adoption of a rake receiver is certainly advisable, to detect and combine the strongest multipath components and to allow for soft handoff. Multipath diversity provides increased quality of service (QoS) through fading mitigation. Conversely, due to the larger free-space loss and on-board RF power scarcity, mobile satellite systems are forced to operate under LOS propagation conditions, at least for medium-to-high data rates. This results in a milder Rice (or at most Rice/log-normal) fading channel [4], with a Rice factor (the power ratio between LOS component and diffuse component) typically ranging between 7 to 15 dB. Multipath diversity in a single satellite link cannot be exploited due to the fact that paths with differential delays exceeding 200 ns most often result have insufficient power to be usefully combined by the rake receiver. Thus fading is effectively nonselective.

Another major difference is that the *useful* dynamic range for the received signal power is much smaller than for terrestrial systems (for which it goes up to 80 dB). This is due to the different system geometry (reduced path-loss variation within each satellite beam, on the order of 3–5 dB) and again to the limited on-board RF power, which is insufficient to counteract path blockage. Path blockage can be induced by heavy shadowing from hills, trees, bridges, and buildings; the car's body and the head of the user can also have a nonnegligible impact. Tree shadowing can lead to 10–20 dB of excess attenuation and is often the cause for link outage. In essence, S-UMTS operates in an *on/off* propagation channel, with Rice fading in the *on* condition [4]. Countermeasures to blockage-induced outage are essential to achieve satisfactory quality of service.

B. Doppler Effect

Doppler effects are of relevance to S-UMTS because of the possible satellite rapid movement with respect to the gateway stations and user terminals. For LEO and most MEO constellations, satellite-induced Doppler is dominating over possible user terminal speed effects. User speed still has a major impact in determining the Ricean fading bandwidth. In fact, the Doppler and delay variations due to the satellite movement relative to the Gateway station can almost be perfectly compensated by means of feed-forward precompensation techniques based on precise satellite orbital position knowledge. This approach allows one to remove the largest Doppler (and Doppler rate) contribution, the feeder link frequency typically operating at C/Ku/Ka frequency band, whereby the carrier frequency is much higher than the S-band user link. Satellite-to-user downlink Doppler can also be removed with feed-forward techniques for the center of each antenna beam, thus leaving the demodulator to deal with the differential Doppler between the center of the beam and its current location. Depending on the beam size, the downlink residual differential Doppler offset amounts to a few kilohertz, i.e., typically less than frequency offset caused by terminal clock instabilities. The downlink satellite carrier frequency differential Doppler can be estimated by the user terminal demodulator, allowing for accurate uplink Doppler precorrection. The latter, jointly with feeder link Gateway precorrection, minimizes the amount of return link frequency uncertainty at the Gateway demodulator input. Techniques to deal with the Doppler effect at demodulator level are briefly discussed in Section II-F.

C. Satellite Diversity

Satellite diversity is instrumental in our S-UMTS design, providing benefits in terms of reduced blockage probability, soft and softer handoff capability, slow fading counteraction, and, under certain conditions, even increased system capacity. First, the intuition that the probability of complete blockage greatly reduces with the number of satellites in simultaneous view recently found confirmation in experimental campaigns [5]. Reference [6] (Fig. 1) shows how in a typical suburban environment the probability of blockage varies with the minimum elevation

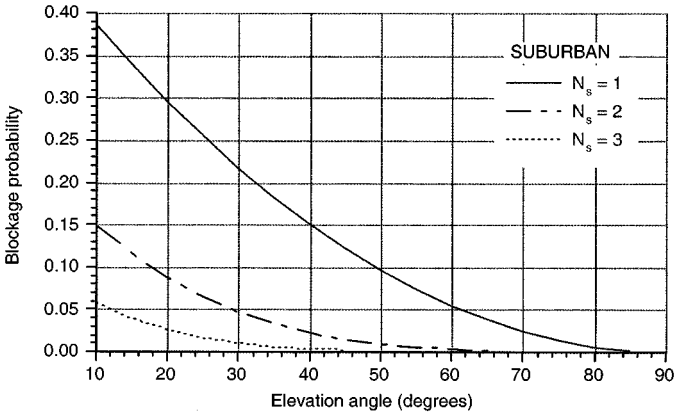

Fig. 1. Path blockage probability in a suburban area, with the number of satellites (N_s) above the minimum elevation angle as a parameter [6].

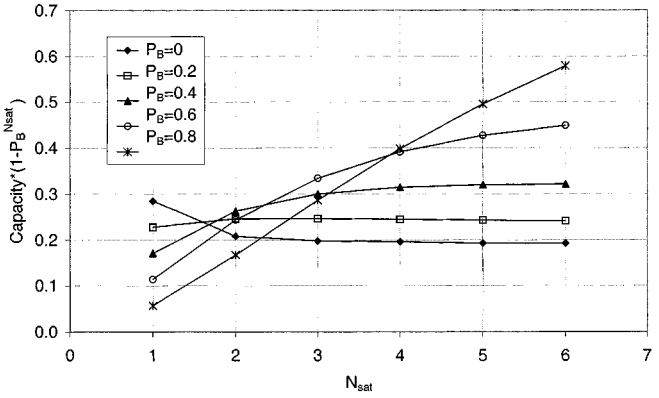

Fig. 2. Product of capacity and probability of at least one clear link versus the number of satellites in visibility [$N_{\rm sat}$], with the single path blockage probability [P_B] as a parameter. Fast Rice fading channel ($K = 10$ dB, 10-ms interleaving delay, speed $= 100$ Km/h), $E_{b,\rm tot}/N_0 = 8$ dB; normalized interbeam interference $\zeta = 0.5$; power control error standard deviation $\sigma = 0.5$. Outage due to power control errors $\gamma = 0.01$.

angle and the number of satellites in view. Reduced blockage translates immediately into improved quality of service. Note that the multiple satellites can be exploited very efficiently in a CDMA system adopting rake receivers to realize soft satellite-handoff and softer spot beam-handoff. CDMA also allows flexible allocation of diversity to different classes of terminals supported by IMT-2000. In fact, fixed or transportable terminals enjoying low blockage probability can be operated without satellite diversity in the FL, thus optimizing network resources exploitation.

Satellite diversity exploitation in the FL has a few differences with respect to the RL that are worth recalling. In the FL, satellite diversity must be forced by the system operator by sending the same signal to different satellites through highly directive antennas. Note that the FL transmitted multiplex can adopt synchronous CDMA with orthogonal spreading sequences. Differently from the terrestrial case, the nonselective satellite fading channel preserves the multiplex orthogonality, thus minimizing intrabeam interference. It should be noted that forwarding the signal through different noncolocated satellites somewhat increases the amount of interbeam interference, thus causing an apparent capacity loss. However, in-depth FL system analysis for a multibeam multisatellite power-controlled CDMA mobile system [6] showed that in practice, for a reasonable probability of single satellite blockage (e.g., 20%, that is, $p_b = 0.2$), the overall system capacity multiplied by the probability of having at least one satellite in view (identified as normalized system capacity) is almost independent from the number of satellites providing path diversity. This result is reported in Fig. 2, from [6], which has been computed for a Rice fading channel with Rice factor $K = 10$ dB, 10-ms interleaving delay, terminal speed of 100 km/h; $E_{b,\rm tot}/N_0 = 8$ dB; interbeam interference normalized to serving beam power $\zeta = 0.5$; power-control error standard deviation $\sigma = 0.5$; and outage due to power control errors $\gamma = 0.01$. Note that for $p_b = 0.4$, satellite diversity provides even larger normalized system capacity. The p_b dependency on the constellation parameters and user environment is very complex and cannot be discussed here. Some experimental results are reported in [4] and [5].

Assuming transparent transponders, exploitation of satellite diversity in the RL is practically unavoidable due to the MT quasi-omnidirectional antenna. Universal frequency reuse allows for *satellite antenna arraying* (similar to deep space probes' ground reception techniques), whereby the different replicas of the same user terminal signal transponded by the different satellites are independently demodulated, time aligned, and coherently combined at the gateway station. This detection technique, requiring a rake receiver, results in a drastic reduction in the user terminal EIRP even under LOS conditions.

As noted in the previous subsection, multipath diversity cannot be exploited in S-UMTS. This fact can seriously affect the link budget, especially for slow-moving MTs. Once more, satellite diversity comes in to yield very significant gains even in the presence of slow fading. This is extremely important, as slow fading is counteracted neither by power control (characterized by very slow dynamic capabilities) nor by the finite-size interleaver. For mobile satellite systems, slow fading represents the most power-demanding link condition. With satellite diversity, it is possible to largely counteract these adverse slow-fading effects with very modest power margins.

In the case of the packet type of traffic, switched diversity is preferable with respect to combining, taking into account the "short" message duration. Still, the satellite path diversity will provide in this case an important advantage in terms of quality of service.

D. Power Control

Considerable attention has been devoted to a fundamental issue for any CDMA system: power control. In fact, although the near–far effect in S-UMTS is not as bad as for T-UMTS, power control must necessarily be implemented in order not to waste precious power and system capacity. Slow (trackable) power-level variations are due to different causes such as satellite motion[1] (path-loss changes), satellite and user antenna gain variations, shadowing, user speed changes, and time-varying

[1]This effect tends to be compensated by the so-called isoflux antenna design that attempts to equalize the geometry-dependent path loss with antenna gain shaping.

cochannel interference. As in T-UMTS, a combination of open-loop for random-access channels and closed-loop power control for connection-oriented channels is required. Due to the longer satellite propagation delay, closed-loop power control is slower and less responsive to fast dynamics as compared to T-UMTS, and as such its design is critical. In the following, we dwell on the implementation of closed-loop power control in SW-CDMA.

Based on the CDMA terrestrial system (IS-95) experience, closed-loop power control can be based on two loops working concurrently to provide the desired FER. The *inner* loop is used to adjust the channel SNIR computed after rake combing and interference mitigation (if applicable) to the target SNIR, which is needed to achieve the target FER. Note that the target SNIR depends on the user bit rate, propagation environment, user speed, and path diversity conditions, all of which change dynamically. Therefore, an *outer* loop is needed to adapt the target SNIR to match the measured FER to the target FER. However, to cope with the increased propagation delay in satellite links, algorithm modifications are required in terms of a) optimization of PCC rate, b) SNIR estimation, and c) mechanization of the inner loop.

Concerning point a), due to the propagation delay, the PCC rate should be reduced to one per frame (10/20 ms, as shown later), as opposed to one per slot, as used in T-UMTS [19], [21]. This avoids oversampling and possible loop instabilities, without affecting the frame structure regularity. Another important point is to keep memory of the last PCCs sent, but not yet received because of propagation delay, before deciding for a new PCC. In this way, power-control tracking of slow variations becomes rather insensitive to the satellite orbital height.

As for point b), SNIR estimation can be performed on the total received signal, or on known reference symbols if available (data-aided). In the absence of reference symbols, two options are available: use tentative, or final, data decisions to remove modulation or use a nonlinear transformation to recover an unmodulated signal component, which can be used in place of the reference symbols (see discussion below). In both cases, a bias in the estimate due to the nonlinear power-estimation process occurs at low SNIR, which however can be compensated for by the outer loop. The variance of the SNIR estimator is more important, and as expected the best results are achieved with the data-aided approach—at the price, however, of some resource expenditure. After detailed tradeoff, it was concluded that a non-data-aided approach was more suitable for the forward link to avoid an excessive overhead for reference symbols (see next section).

Concerning point c), a four-level inner loop mechanization can be shown to provide the best tracking performance in most situations. The four levels correspond to small/large, positive/negative steps. The small step is well suited to track, with minimum jitter, "regular" changes in antenna gain or path loss and slow shadowing, while the large step is best suited to recover sudden changes in the received SNIR.

1) SNIR Estimator Mechanization:

a) Data-aided approach: Denote with $z_i, i = 1, \ldots 16$, the received reference symbols samples. We assume that $+1$ reference symbols are transmitted and that frequency, but no phase correction, has already been applied on the received symbols.

Then the estimated SNIR is the ratio of the two quantities below

$$S = \left[\sum_{i=1}^{16} z_i m_i^*\right]^2$$

$$N + I = P_T - S = \sum_{1}^{16} |z_i m_i^*|^2 - S$$

where P_T is the total estimated power and m_i is the average signal phasor computed by the channel estimator unit for the interval centered around z_i. The length of such interval is itself a parameter to be optimized taking into account the expected channel dynamic. An alternative would be to compute the noise floor directly as

$$N = \sum_{i}^{16} |m_i^*(z_i - m_i)|^2.$$

For simplicity, here only the case of no diversity is considered, since the generalization to multiple diversity is straightforward [35]. Taking into account that the noise (plus interference) floor is changing quite slowly, an average of successive noise power measurements with a first-order recursive filter is feasible [35]. This approach has been selected for the reverse link.

b) Non-data-aided approach: In the absence of reference symbols, the SNIR can still be estimated according to the above procedure, with the only change that the sample z_i then refers to the signal samples after passing them through nonlinear function $f(\,)$. A possible nonlinear transformation for a QPSK modulated signal is $f(re^{j\varphi}) = re^{j4\varphi}$. There is no claim, however, that this is the optimum nonlinearity. For low SNIR ratios, the $f(re^{j\varphi}) = r^2 e^{j4\varphi}$ nonlinearity is likely a better choice.

c) Decision-directed approach: Alternatively to NDA, a decision-directed approach can be selected in which the samples z_i are rotated according to a tentative (before decoding) or final (after decoding) decision about the corresponding transmitted symbol. Clearly, waiting for final decisions would increase the loop delay, but this could be acceptable in MEO/GEO S-UMTS systems where propagation delays might be larger than decoding delay.

Detailed simulation results, however, indicated that for the forward-link case (where reference symbols are typically not available), the nonlinear transformation method is preferable, as it slightly outperforms the decision-directed approach (with both final and tentative decisions).

2) Inner Loop Mechanization: In the case of a four-level command, the inner loop can be mechanized as follows. Define $\varepsilon_0 = \mathrm{SNIR}_{\mathrm{meas}} - \mathrm{SNIR}_{\mathrm{target}}$ (all parameters in dB); Δ_1^{PC} and Δ_2^{PC} as the small and large power-control steps; and $N_1^{\mathrm{UP}}, N_1^{\mathrm{DW}}$, and $N_2^{\mathrm{UP}}, N_2^{\mathrm{DW}}$ as the numbers of small and large up and down PCs sent in a period equal to N_d frames (N_d being the loop delay expressed in frames). Then, letting ε_1 (dB) be the error threshold for sending a large power-control step Δ_2^{PC}, compute $\varepsilon_c = \varepsilon_0 + (N_1^{\mathrm{UP}} N_1^{\mathrm{DW}})\Delta_1^{\mathrm{PC}}(N_2^{\mathrm{UP}} - N_2^{\mathrm{DW}})\Delta_2^{\mathrm{PC}}$.

- If $|\varepsilon_c| < \varepsilon_1$, send an up correction Δ_1^{PC} if $\varepsilon_c < 0$ and a down correction if $\varepsilon_c > 0$.

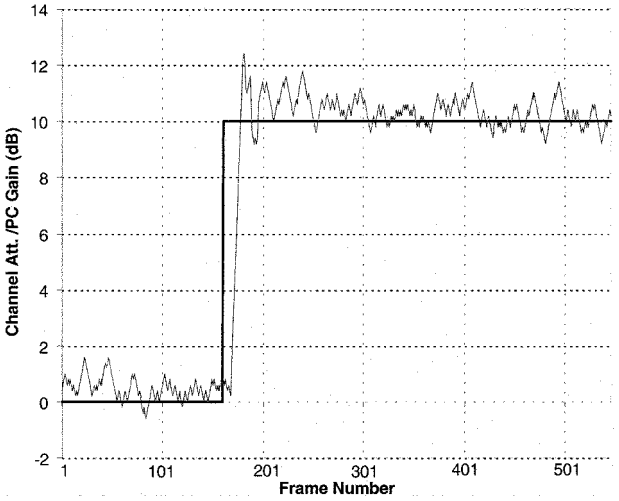

Fig. 3. Power-control loop response to a 10-dB step path attenuation (AWGN channel). Overall (two-way) loop delay is 120 ms. Four-level PC loop with NDA SNIR estimate. $\varepsilon_1 = 2$ dB, $\Delta_1^{PC} = 0.2$ dB, $\Delta_2^{PC} = 1$ dB, $G_{\rm dw} = 0.002$ dB, $G_{\rm up} = 0.02$ dB, $N_d = 5$. Target FER was 10^{-2}.

- If $|\varepsilon_c| > \varepsilon_1$, send an up correction $\Delta_2^{\rm PC}$ if $\varepsilon_c < 0$ and a down correction if $\varepsilon_c > 0$.

For the case of a three-level PC strategy, simply set $\Delta_2^{\rm PC} = 0$. The two-level PC corresponds to $\varepsilon_1 = \infty$.

3) Outer Loop Mechanization: The outer loop updates the target SNIR in a way similar to that of terrestrial systems, according to the following algorithm.

- If the received frame is correct, then decrease the target SNIR by the quantity $G_{\rm dw}$
- If the received frame is wrong, then verify how many target SNIR up corrections have been done in the last N_d frames (N_d being the loop delay expressed in number of frames). If (number of up corrections in last N_d frames $>$upMax), do nothing; else increase the target SNIR by the quantity $G_{\rm up}$.

4) Simulation Results: After intensive simulations, the following parameters have been selected: threshold for large power-control step $\varepsilon_1 = 2$ dB, small step for SNIR errors less than ε_1 : $\Delta_1^{\rm PC} = 0.2$ dB, large step for SNIR errors greater than ε_1 : $\Delta_2^{\rm PC} = 1$ dB, outer loop down step $G_{\rm dw} = 0.002$ dB, outer loop up step $G_{\rm up} = 0.02$ dB, and $N_d = 5$. Figs. 3 and 4 show the response to a step attenuation and to a sinusoidal attenuation variation when the overall loop delay amounts to 120 ms and the frame length is 20 ms. The conservative 120-ms two-way delay accounts also for processing delay in addition to pure propagation delay. Note that the step response is representative of sudden signal variations due to link obstructions. The sinusoidal [in dB] signal power variations are representative of smooth signal power-level changes due to the satellite or user movement and consequent antenna gain variations or specular multipath for a slowly moving user. In both cases, the loop corrections (thin line) appear to well counteract[2] the "slow" channel attenuation variations (thick line). Further, Fig. 5 shows that the performance of power control is quite insensitive to the actual loop delay. This result was obtained for a two-level loop but applies also to the four-level loop.

Lastly, we want to quantitatively confirm the limitations and capabilities of power control in S-UMTS. Table I shows the average RP requirement needed to achieve a target FER of 10^{-2} with and without power control, in the presence of fast Rice fading superimposed to a slow sinusoidal shadowing (± 5 dB peak-to-peak). The RP requirement is representative of the power needed on-board (in the FL case) or at the user terminal (in case of reverse link) for a given channel to provide a given FER performance. The RP is actually equivalent to the average E_b/N_o for cases without power control and with Ricean fading only. The simulation results confirm that in S-UMTS, power control is only partly able to track fading fast power variations, and as such there are moderated gains in average requested RP with respect to a non-power-controlled system. However, if power control is not implemented, the requested RP must be achieved through the systematic use of static link margins, which must therefore be sized for the worst case attenuation. Instead, adaptive power control is capable to detect unacceptable link quality of service and promptly correct for it with an adequate average power increase *only when it is required*. In essence, power control is essential in S-UMTS systems to minimize the power-control dynamic link margins and to avoid capacity degradations induced by the systematic use of static link margins. It should be noted that for non-real-time services such as packet-based applications depending on MT, pilot SNIR reports the system can decide to delay transmission of packets to a better time instant from the link quality point of view.

E. Pilot Channel

A pilot channel is useful in both FL and RL. Considering the FL, first note that the (fast) satellite motion in LEO/MEO/HEO constellations generates a remarkable Doppler effect that must be accounted for in the system design. The main Doppler impact is the need for special measures for initial signal acquisition and carrier tracking. Most of the Doppler can, however, be precompensated for, thus reducing the frequency uncertainty at least for the feeder link part (satellite-to-gateway) and for the downlink center-of-beam. To ease initial pseudonoise sequence synchronization, it is expedient to include in the satellite FL a common pilot, which can also be used to achieve coherent detection and to initially adjust the power level in the return direction (open-loop power control). Also, time-domain multiplexing of pilot symbols (TDMP) in the different data streams in preassigned time slots is a possible option to support adaptive satellite antennas.

In the RL, a pilot can be paired to each information signal. The reduction in power level (around 10–20% power on pilot is typical) is balanced by the benefit of coherent detection at the gateway [7]. Code-division multiplexing of an auxiliary channel carrying pilot symbols and signaling information (rate information, power control bits) (CDMP) was found preferable from the system perspective. In the RL, pilot-aided CDMA quasi-coherent uplink was found to provide a gain higher than 1 dB compared to the 64-ary noncoherent Walsh–Hadamard keying modulation used for second-generation cellular and satellite voice

[2]Note that in case of sinusoidal power variations, for plot clarity the inverse of the power-control gain is plotted against time.

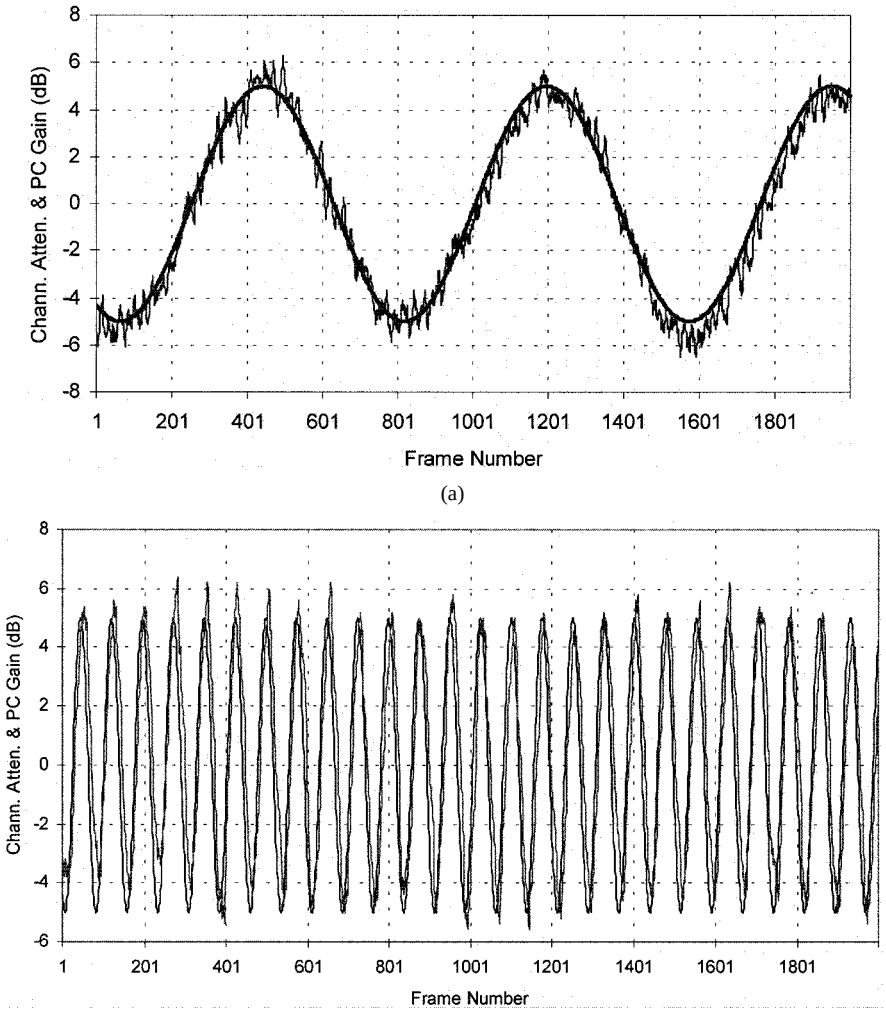

Fig. 4. Response of power control to a 10-dB peak-to-peak sinusoidal attenuation [frequency 0.1 (a) and 1 Hz (b)]. AWGN channel. Overall (two-way) loop delay is 120 ms. Four-level PC loop with NDA SNIR estimate. $\varepsilon_1 = 2$ dB, $\Delta_1^{PC} = 0.2$ dB, $\Delta_2^{PC} = 1$ dB, $G_{\rm dw} = 0.002$ dB, $G_{\rm up} = 0.02$ dB, $N_d = 5$. Target FER was 10^{-2}.

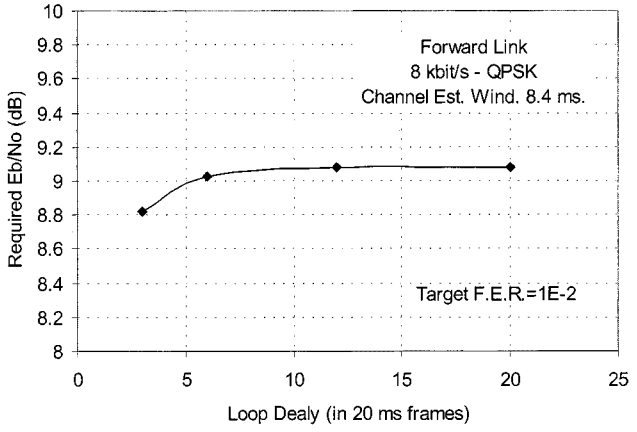

Fig. 5. Required E_b/N_0 for FER $= 10^{-2}$ as a function of the loop delay. Slow Ricean fading case (Doppler spread $= 6$ Hz). Bilevel power control with NDA SNIR estimate. $\varepsilon_1 = 0$ dB, $\Delta_1^P = 0.5$ dB, $\Delta_2^P = \infty$ dB, $G_{\rm dw} = 0.002$ dB, $G_{\rm up} = 0.02$ dB, $N_d = 5$. Target FER was 10^{-2}.

networks even at very low symbol rates (up to 2.4 kbit/s) [7]. The quadrature pilot symbols' insertion (together with control channel bits) allows one to independently transmit variable-rate traffic from control signaling and pilot symbols with reduced envelope fluctuations.

F. Code Acquisition

In the FL, the system must guarantee efficient initial code acquisition at the mobile terminal, both for log-in into the system and for soft handoff handling. As pointed out in the previous Section II-E, a common pilot tone can be introduced for this purpose. The pilot tone can be in the form of a CW spread by a long PN code, as in IS-95, or as a BP, where all the pilot energy is concentrated in a fraction d of the available slot time, identified as the *duty cycle*. Evidently, for the same average pilot power, the peak power for BP is $1/d$ times higher than for CW. We analyzed both approaches, adopting various versions of the maximum/threshold crossing (MAX/TC) criterion [8] to drive the acquisition subsystem. In all cases, noncoherent postdetection integration is needed to achieve sufficient SNR to make reliable decisions. Also, a single dwell architecture was assumed for simplicity. Fig. 6 shows the mean time to acquisition using the TC criterion for the FL pilot evaluated as a function of the chip energy to thermal noise density E_c/N_0. The computation

TABLE I
AVERAGE RELATIVE POWER (S) REQUIREMENT WITH A 10-dB PEAK-TO-PEAK ($A_{\rm pp}$) SINUSOIDAL VARIATION (FREQUENCY 0.1 Hz). AWGN CHANNEL. LOOP DELAY IS 100 ms. LOOP PARAMETERS AS FOR FIG. 3 (FOUR-LEVEL PC) AND FIG. 5 (TWO-LEVEL PC). FOR REFERENCE, A CASE WITH $A_{\rm pp} = 0$ IS ALSO SHOWN. FRAME LENGTH IS 20 ms AND DATA RATE IS 8 kbit/s (CONVOLUTIONALLY ENCODED WITH RATE 1/3, $k = 9$ CODE)

Loop Characteristics	SNR Est.	S (dB)	FER	BER
No Power control	N/A	7.46	1.0E-02	5.2E-04
BiLevel Loop. Gain Step=0.5 dB	DA	6.46	1.02E-2	7.9E-4
BiLevel Loop. Gain Step=0.2 dB	DA	5.76	9.94E-3	5.77E-4
BiLevel Loop. Gain Step=0.5 dB	NDA	5.66	9.91E-3	5.73E-4
BiLevel Loop. Symbols, Gain Step=0.2 dB	NDA	5.18	9.90E-3	4.57E-4
4-Lev. Loop. Gain Step=0.2 / 1 dB	DA	5.97	1.01E-2	6.98E-4
4_Lev. Loop Gain Step=0.2 / 1 dB	NDA	5.06	9.9E-3	4.54E-4
BiLevel Loop. Gain Step=0.5 dB (A_{pp}=0.)	NDA	4.0	9.90E-3	5.39E-4
4_Lev. Loop Gain Step=0.2 / 1 dB (A_{pp}=0.)	NDA	3.49	9.9E-3	4.24E-4

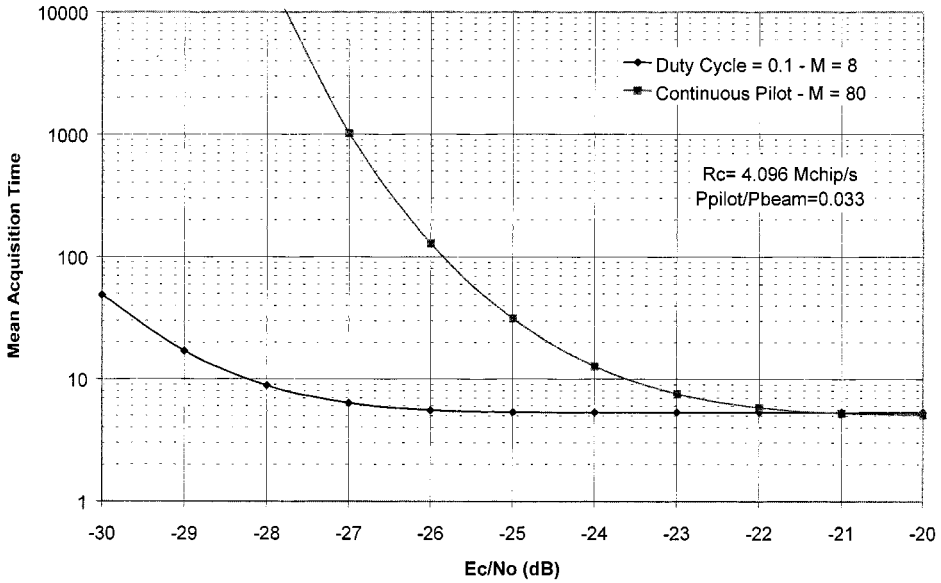

Fig. 6. FL mean acquisition time (ms) versus pilot thermal E_c/N_0 for a continuous and bursty pilot. Average pilot power equal to 3.3% of the total beam power. M is the number of noncoherent post integrations. The assumed duty cycle for the bursty pilot corresponds to one code period out of ten transmitted.

assumes that the user is at the crosspoint of three equal loaded beams and that in each beam, only 3.3% of the beam power is dedicated to the pilot.

Coherent integration over 256 chips was assumed with subsequent noncoherent postintegration (indicated by M in figure) equal to 80 and 8, respectively, for the CW and bursty pilot cases. A maximum frequency error of 20 kHz was considered in the performance analysis. To cope with the frequency error, a matched filter processor has been considered with a parallel frequency search through the use of the swivelled FFT concept [9]. This is equivalent to searching in parallel for the correct code epoch on different signal replicas, each one frequency shifted with respect to the original one by a multiple of the FFT frequency resolution. In practice, not all FFT frequency bins have to be computed, and further HW simplification may be achieved by using approximated sine and cosine FFT base functions with negligible impact on performances. Actually, a three-value (± 1 and 0) representation of the FFT sine and cosine basis functions would represent the best compromise between performance and HW complexity. Fig. 6 shows a definite advantage for the BP solution, which can be explained by the fact that, assuming equal dwell time for BP and CW, more energy is integrated *coherently* in the BP case. However, it can be shown that allowing for a longer noncoherent postdetection integration in CW (approximately double with respect to BP), the same sdetection probability can always be achieved. In essence, there is a tradeoff [10] between acquisition time (which is in favor of BP, but not dramatically) and hardware complexity and resilience to nonlinearity (which are in favor of CW). In our system simulations, reported in Section IV, we have adopted the BP approach.

Coming now to consider the RL, the main difference is that for power-efficiency reasons, no individual high-power pilot as in the FL can be permanently transmitted for acquisition purposes. Initial code acquisition shall instead be performed on a single ad hoc preamble, which is transmitted only once. Furthermore, a TC strategy should be adopted (a MAX strategy requires that there is always a right hypothesis to detect), and sophisticated multiple-dwell algorithms cannot be exploited. An ML strategy could be adopted, if the presence of the burst has been previously detected with another strategy [11]. Another important difference is that more hardware complexity can be supported in the gateway. Again, frequency errors and possibly timing errors must be faced. A strategy, similar to the FL approach, is to coherently integrate on a partial number of chips

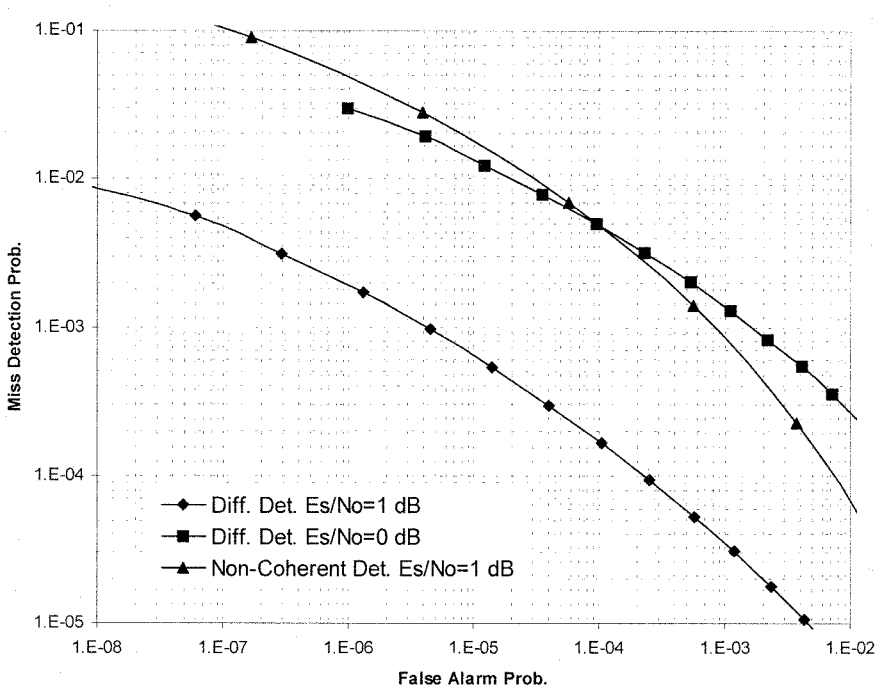

Fig. 7. Receiver operating characteristic (ROC) for differential detection of a 48 symbols UW. $E_s/(N_0 + I_0)$ equal to 0 and 1 dB. Also shown is the ROC for noncoherent detection over 49 symbols.

S_k, and then complete by noncoherent integration, adding the squared envelope of the $N_{\rm nc}$ partial correlations $\sum_{k=1}^{N_{\rm nc}} |S_k|^2$. An alternative strategy is to substitute noncoherent integration, with differential integration $\sum_{k=2}^{N_{\rm nc}} S_k S_{k-1}^*$. A comparison between the two strategies, in terms of false-alarm probability and missed-detection probability, is shown in Fig. 7. It appears that differential integration yields the best results, and this was adopted in our simulations.

G. Digital Modulation and Spreading Format

A large effort has also been devoted to the optimization of modulation and spreading format. For the FL, three options were considered:

1) QPSK modulation with binary Walsh–Hadamard (WH) spreading and real binary scrambling (option Q) ;
2) dual BPSK with WH spreading and complex scrambling (option D);
3) BPSK modulation and WH spreading, with half of the user carriers being transmitted on the in-phase channel and the other half on the quadrature channel, and I and Q scrambled by two different codes (option IQ).

An asymptotic analysis has been performed using both a conventional correlation receiver, also identified as an SUMF receiver, and an ideal interference-suppressing LMMSE receiver. Implementation of interference mitigation in S-UMTS will be described in more detail in the next section. In both cases, ideal coherent detection is assumed. Results are given in Fig. 8, where the cumulative distribution for SNIR obtained at the receiver output is shown. The nominal SNR (thermal noise only) is 6 dB in all cases. Both double-diversity (thick lines) and triple-diversity (dotted lines) with maximal ratio combining were considered, with each satellite carrying the same K number of users (all at equal level). The spreading factor considered for IQ was 64. For Q and D, the spreading code length is actually doubled, due to the longer symbol interval. Note that for SUMF, the three schemes achieve the same average SNIR. However, the SNIR distribution for D has slightly shorter tails than that for Q, while IQ has the longest tails. With an LMMSE receiver, Q performs significantly better than D and IQ, with the advantage increasing with the number of users. The reason is that Q has a double spreading code length with respect to IQ and requires half the number of codes required by D. A remarkable result is that triple satellite diversity provides better SNIR under light loading conditions, while in high loading conditions, the best SNIR is achieved with double diversity. In our proposal, the Q option was selected for data rates larger than 4.8 Kb/s. For very low data rates (i.e., 2.4 Kb/s), BPSK is recommended as simulations indicated its superiority when channel estimation errors and user terminal phase noise are considered. As the for SUMF, the difference between QPSK modulation with real and complex spreading (not shown here) is basically nonexistent. We propose for the modulation and spreading baseline the latter, i.e., the same T-UMTS solution. However, for the optional case in which short (256 chips long) scrambling sequences are selected, option Q is recommended to maximize LMMSE advantages.

H. Interference Mitigation

For a multisatellite SW-CDMA system exploiting path diversity, the capacity bottleneck is represented by the FL. This is due to the limited satellite RF on-board power available, which hurts FL capacity, and to the (quasi)-permanent uplink soft handoff

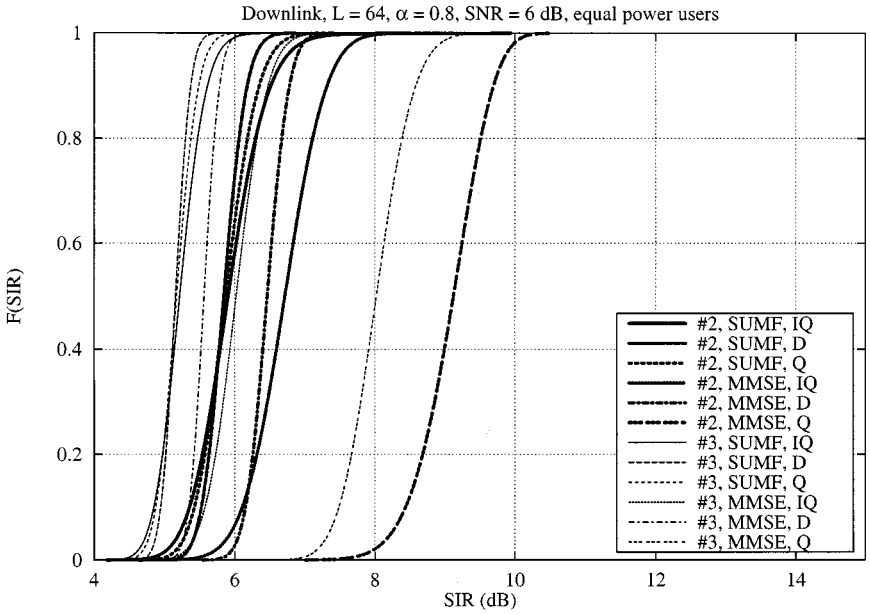

Fig. 8. FL SIR cumulative distribution function. Number of users/spreading factor $= 0.8$.

conditions that increase RL capacity. This explains our interest for robust decentralized CDMA interference mitigation techniques that can be applied to the mobile user terminal, thus reducing average FL power consumption. Among the different CDMA interference mitigation techniques, the blind MOE solution [12]–[14] appears particularly suited for use in a decentralized single detector implementation because of the affordable complexity increase compared to the conventional correlation receiver (CR) [15]. Nonlinear schemes were discarded for their complexity, which was not suited for a single user terminal, and sensitivity to channel estimation errors. More precisely, the scheme investigated was the EC-BAID [14] featuring an extended observation window, rotational phase invariance allowing for carrier phase removal after the adaptive detector, and insensitivity to interferers' frequency offset. Both LMS and RLS EC-BAID adaptation schemes were simulated. However, the RLS version suffers from a much greater implementation complexity compared to LMS. The marginal RLS advantage over LMS provided in AWGN channel was found to be superseded by the superior LMS performance over fading channels [3]. The LMS version is the one considered in the numerical results.

I. Resource Allocation

An important system issue is the selection of a strategy for resource allocation in a system using a satellite constellation and in which satellite beams can overlap. This issue must be seen in conjunction with the potential advantages provided by the MOE adoption. Three different strategies have been considered for FL resource assignment.

1) Avoid frequency reuse among overlapping satellites adopting CDMA/FDMA multiplexing.
2) Full frequency reuse among all beams of all satellites without applying permanent satellite path diversity[3].
3) Full frequency reuse among all beams of all satellites applying permanent satellite diversity (soft handoff).

Clearly option 1) is the one minimizing mutual satellite interference at the expense of the occupied bandwidth. In fact, when no frequency reuse among satellites is implemented, then FDMA satellite multiplexing implies an increased bandwidth occupancy compared to a full frequency reuse scenario. Option 2) avoids the CDMA/FDMA bandwidth increase at the expense of an increased intersatellite CDMA self-noise. It should be recalled that for an individual satellite, the intrabeam interference is eliminated by the adoption of orthogonal CDMA at beam level. Option 3) combines the frequency reuse advantage of option 2) with the artificial path diversity generation achieved by using multiple satellites, as described previously. Disregarding blockage effects, semianalytic simulation results for the case of slow-fading encountered by hand-held terminals have been found in [16]. Considering as a figure of merit the number of active users/frequency slot/beam/satellite, which accounts for both power and spectral efficiency, it has been found that option 3) is preferable for both CR and MOE detectors while the adoption of MOE detectors instead of a CR provides a 110% capacity increase for option 2), 60% for option 1), and 50% capacity boost for option 3). The MOE advantage will be even more important in a practical system, whereby power-control errors will enhance the multiple-access interference effects.

III. SW-CDMA Versus Terrestrial W-CDMA Specifications

As repeatedly stated, SW-CDMA represents an adaptation of the T-UMTS W-CDMA proposal [17]. For this reason, only the main SW-CDMA features and deviations from W-CDMA

[3]Temporary satellite path diversity can be envisaged during satellite handoff.

TABLE II
MAPPING OF LOGICAL CHANNELS TO PHYSICAL CHANNELS

Logical Channels	Link direction	Physical Channels
Broadcast Control Channel (BCCH)	Forward	Primary Common Control Physical Channel (Primary CCPCH)
Forward Access Channel (FACH) Paging Channel (PCH)	Forward Forward	Secondary Common Control Physical Channel (Secondary CCPCH)
Random Traffic Channel (RTCH)	Forward	Physical Downlink Shared Channel (PDSCH)
Random Access Channel (RACH) Random Traffic Channel (RTCH)	Reverse	Physical Random Access Channel (PRACH)
Dedicated Control Channel (DCCH)	Forward/Reverse	Dedicated Physical Data Channel (DPDCH)
Dedicated Traffic Channel (DTCH)	Forward/Reverse	Dedicated Physical Data Channel (DPDCH)
Layer 1 signaling	Forward/Reverse	Dedicated Physical Control Channel (DPCCH)

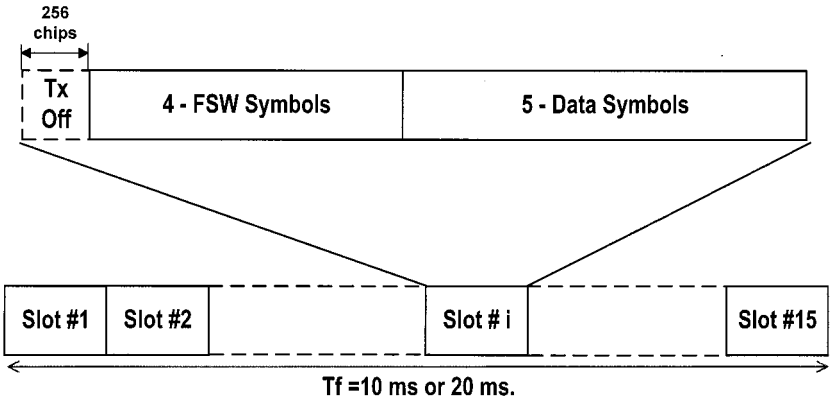

Fig. 9. Primary common control physical channel.

will be discussed here. As the T-UMTS specifications are still evolving, the discussion here mainly refers to the T-UMTS RTT specifications at the time of approval by ITU.

A. Chip Rate

In SW-CDMA, two chip-rate options are supported: a 3.84-Mchip/s baseline and a half-rate option at 1.92 Mchip/s, which may be more suitable in a multioperator environment where bandwidth limitations may arise.

B. Channelization and Scrambling Codes

As in W-CDMA, FL channelization is based on the OVSF codes [22] to accommodate different data rates while maintaining orthogonality. OVSF codes efficiently support frame-to-frame variable bit rates without requiring an increase in demodulator hardware complexity (no need for multicode correlators for higher data-rate services). OVSF is also used in the RL to multiplex the various data and signaling channels transmitted by the user. The same T-UMTS 38400 chip (one frame long) randomization complex spreading code is proposed in case no forward-link mitigation techniques are adopted [20]. A major difference with respect to W-CDMA is the *optional* use of a short randomization (scrambling) code (an extended Gold-like code of length 256 chips) to exploit the benefits arising from the use of adaptive linear interference mitigation techniques, as discussed in the previous section.

C. Logical Channels

The set of logical channels used in SW-CDMA and the supporting physical channels is listed in Table II. The logical channels are the same as those defined in Recommendation ITU-R M.1035 apart from the Layer 1 signaling channel. This logical channel has the purpose of supporting coherent demodulation, power-control functions, and data-rate agility. It is mapped to the DPCCH[4] and is always associated (via time or code multiplexing) to at least one DPDCH.

The CCPCH is available on the FL (see Fig. 9). In particular, a primary CCPCH will carry the broadcast control channel (BCCH) and a frame synchronization word (FSW). The primary CCPCH has a fixed transmission rate (15 kbit/s in the full-chip-rate option and 7.5 kbit/s in the half-chip-rate option). The primary CCPCH is idle at the beginning of each slot for the duration of one symbol (256 chips). During this interval, a bursty pilot called the SCH is transmitted. Such a bursty reference symbol is used mainly to support initial code epoch (and slot timing) acquisition, but it can also be exploited for performing coherent demodulation of CCPCH and DPDCH/DPCCH. Differently from T-UMTS [18], the SCH uses the same scrambling code as the primary CCPCH and is therefore orthogonal to all other FL channels belonging to the same beam. Even in case the long scrambling code option is selected, always the same 256 chips are used by the SCH, thus reducing initial acquisition HW complexity. The transmission power associated to the SCH is typically higher than that of the primary CCPCH to facilitate initial acquisition.

As for T-UMTS [18], to support efficient packet transmission of the FL, a PDSCH is envisaged. The PDSCH can be quickly reallocated to different users in each successive frame. This avoid the need to permanently allocate to a user

[4]The logical Dedicated Control Channel (DCCH), which has the purpose of supporting layer 2 and higher signalling functions, is instead multiplexed with the dedicated traffic channel (DTCH) on the same DPDCH.

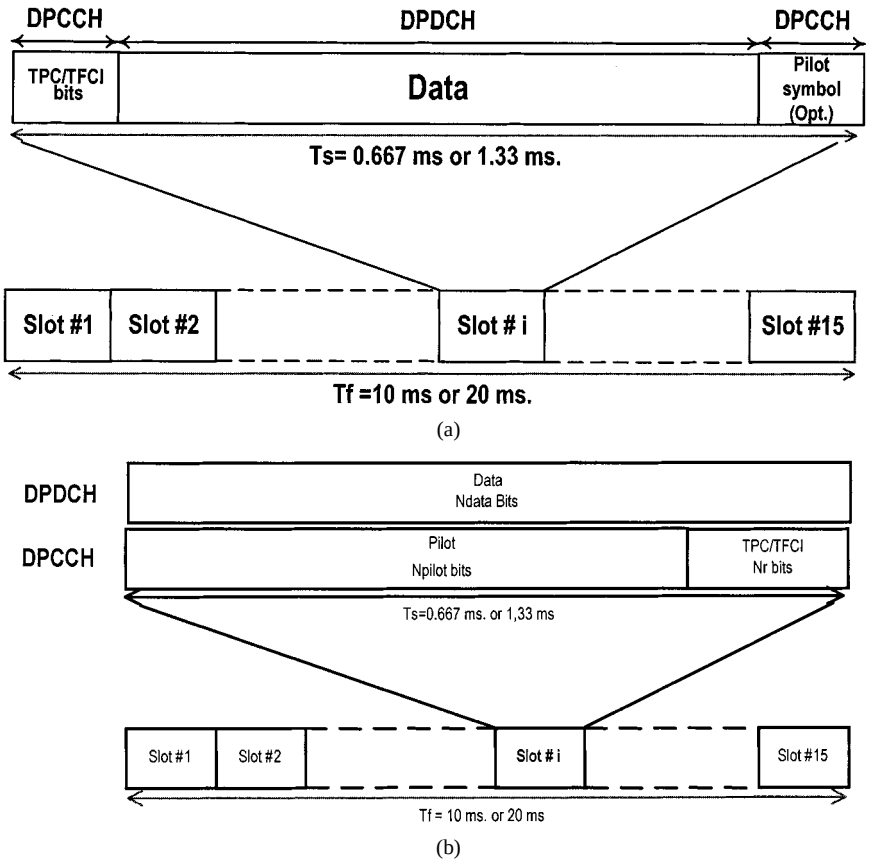

Fig. 10. Frame structure of the (a) forward- and (b) return-link dedicated physical channels (DDPCH/DCPCH).

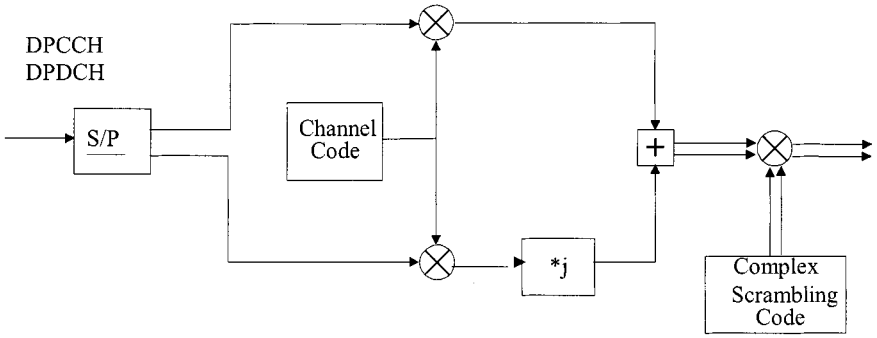

Fig. 11. FL modulation and spreading.

a DPDCH/DPCCH, which would only be used for a small percentage of time due to the packet nature of the requested service. In such a case, in fact, code exhaustion could be experienced well before saturating the potential system capacity.

D. Frame Structure

Fig. 10(a) shows the FL frame structure for the DPDCH and DPCCH; the two logical channels are time multiplexed within each of the slots comprised in a frame. Each DPCCH may actually be split into two parts (respectively transmitted at the beginning and end of each time slot): the first part supports the transmission of TPC commands and TFCI; the second part is optional and only used when on-board adaptive beam-forming is used. In such a case, reference pilot symbols need to be transmitted within each DPCCH to support coherent demodulation. The frame length is 10 or 20 ms when the half-chip-rate option is adopted. The FL modulation and spreading adopts QPSK modulation with binary spreading and scrambling codes (see Fig. 11), as per our system engineering study.

Coding of TPC and TFCI is such that one separate TPC and TFCI command is transmitted per frame. The TPC/TFCI information is block encoded using a Reed–Muller code as for T-UMTS W-CDMA [19]. Here a lower coding rate is proposed to enhance DPCCH efficiency for low-bit-rate applications. This allows one to reduce the overhead power associated to the DPCC transmission. Hence, the up/down power-control command rate is reduced compared to W-CDMA to a single command/frame. Fig. 10(b) shows the frame structure for the RL DPDCH and DPCCH channels. The RL modulation and spreading format is depicted in Fig. 12. Similarly to T-UMTS [20], the DPDCH and the DPCCH are code multiplexed and phase multiplexed. This approach, combined with complex

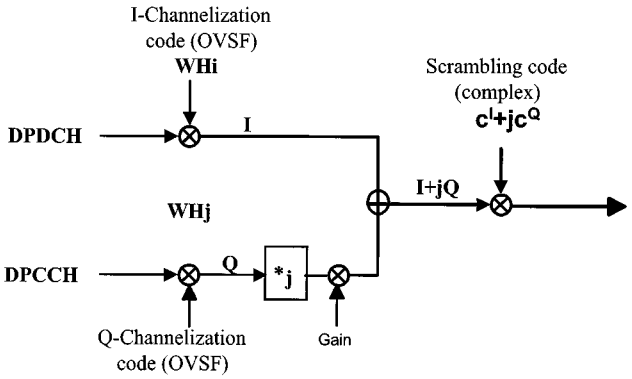

Fig. 12. RL modulation and spreading.

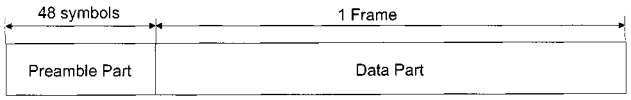

Fig. 13. PRACH channel structure.

scrambling, helps in reducing carrier envelope fluctuation even with unbalanced I and Q power level.

E. Packet Service

In the FL, packet traffic is supported either on the FACH channel for sporadic packets or on a dedicated traffic channel, possibly complemented by a shared channel (the PDSCH), for intense packet traffic. The main advantage of this last approach is that a high-speed common pipe can be shared among active users while the closed-loop power control can be kept active through a low-rate DCH associated channel during the inactive time slots, thus minimizing packet service interference to the other active channels in the same frequency slot. The associated DCH channel is released when not required, i.e., during the reading time between Web page download. In the RL, the RACH channel may be utilized for the transmission of occasional short user packets, mapped onto the PRACH. The PRACH is composed by a 48 quaternary symbol preamble and a data part whose length is one frame (Fig. 13). The preamble part is spread by a binary code, which is randomly selected between a limited set of codes for random access. The usable set of codes is communicated on the BCCH channel. The PRACH burst data part is actually composed of a data channel on the I transmission arm, an associated control channel on the Q transmission arm carrying the reference symbols for coherent demodulation, and an FCH informing about the data rate and format of the I arm. The PRACH burst data part spreading is complex and similar to the spreading of normal dedicated carriers. The I and Q codes used are univocally associated to the binary code used for spreading the preamble. For a nonoccasional but still moderate throughput and/or low duty cycle packet traffic, ad hoc codes will be assigned by the gateway to the user in order to avoid code collision with other users of the RACH channel. In this case, the random traffic channel is still mapped on a RACH-like physical channel. The data part, however, may be of variable length (in any case a multiple of the physical layer frame length). For higher throughput packet channels on the RL, a couple DPCCH/DPDCH can be assigned. The DPDCH is only transmitted when the packet queue is not empty. In this case, in addition to the advantage of keeping the closed-loop power control active during packet bursts, the channel allocation approach allows one to keep full channel synchronization.

IV. Physical Layer and Source Coding Performance Simulation

A complete physical-layer simulator program was developed to accurately simulate the proposed RTT performance. Considering the high SNR affecting the feeder links (gateway–satellite link), only the user links (i.e., from satellite to user and vice versa) have been modeled. The simulator is capable of accurately modeling both the FL and the RL. The following aspects of the physical layer have been modeled: signal framing structure, FEC coding and puncturing, interleaving, modulation and spreading (for traffic and signaling channels), CDMA interference (from the various satellites), channel impairments (HPA nonlinearity, carrier/code Doppler, phase noise, Ricean fading), satellite diversity, and multirate rake demodulators (inclusive of initial acquisition, chip tracking, frequency, phase and amplitude estimators, CDMA interference mitigation, deinterleaving FEC decoders). Only a few aspects of the real system have not been included in the simulator due to their excessive impact on the required simulation time. The most notable omission is the power-control loop. Validation of the power-control loop was performed with a different simplified ad hoc simulator, the results of which have been discussed in Section II. In all simulations, if not otherwise stated, flat Rice fading channel with a Rice factor (indicated with C/M on the following figures) of 10 dB was assumed. Two different user speeds were considered: 70 and 3 Km/h, corresponding, respectively, to Doppler spreads of 140 Hz (FF) and 6 Hz (SF) assuming operation in the 2-GHz IMT-2000 band. The Doppler spread associated to each performance curve shown in this paper is indicated by the parameter Bm (band of multipath) reported in each figure.

Finally, it shall be mentioned that in order to reduce the simulation time most of all, the physical-layer simulation results here shown were obtained with a chip rate equivalent to that of the S-UMTS half-rate option. In addition, the physical-layer simulator was coupled to various traffic generators to perform an end-to-end source coding simulation.

A. Forward-Link Physical-Layer Performance

A high-level block diagram of the forward-link simulator is shown in Fig. 14. For each simulated satellite, the CDM corresponding to each beam —composed by a primary CCPCH (i.e., the pilot carrier) and a number of traffic channels—is independently generated. The CDM multiplex corresponding to the different satellite beams is then summed together. The resulting multibeam satellite envelope is going through an HPA and then through a channel simulator. It has been shown in [23] that the single HPA represents a worst case modeling of the on-board nonlinearity effects experienced by a CDMA signal flowing through an active phased-array antenna. Signals generated by the different satellites, affected by different delay, Doppler, and

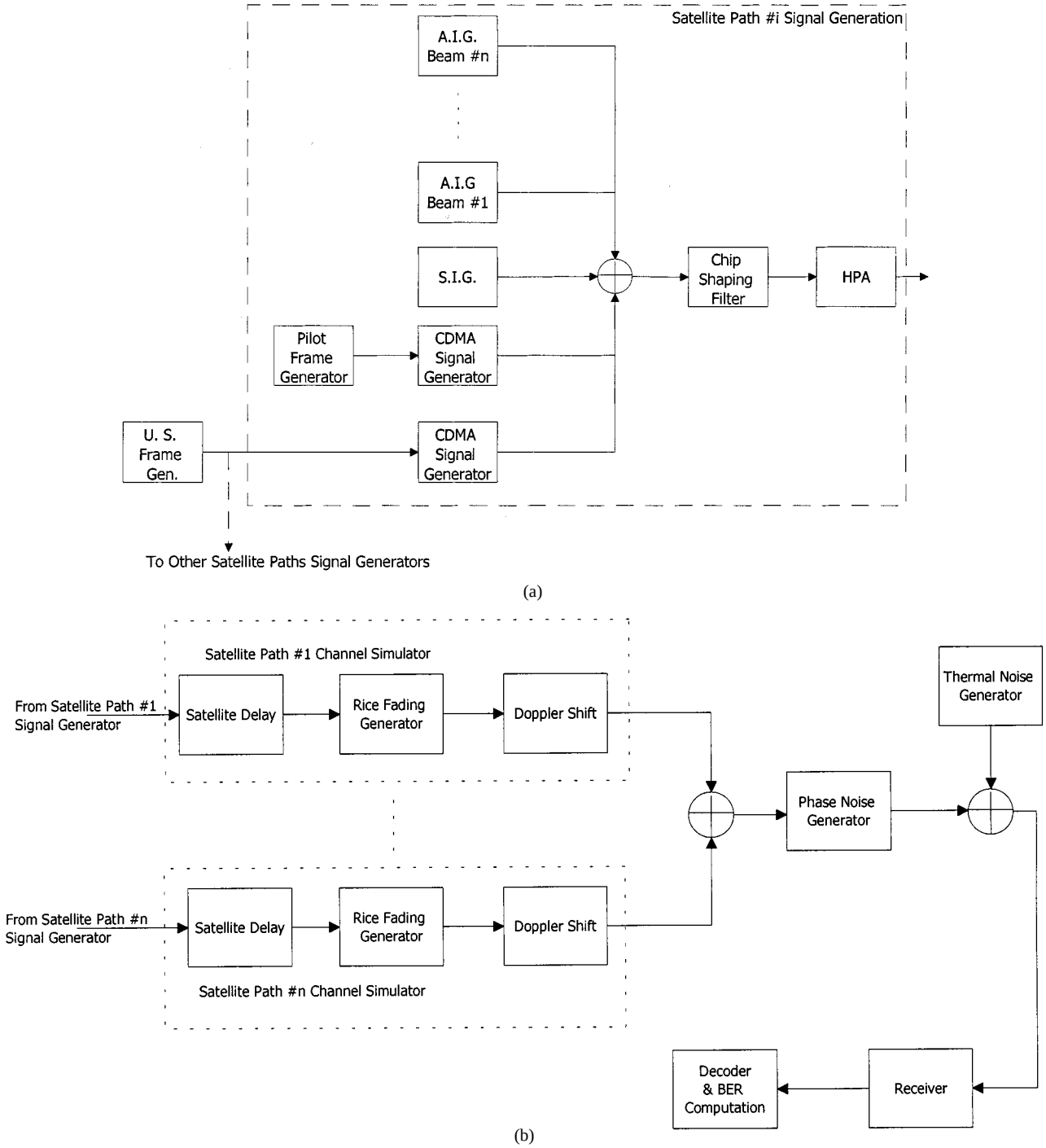

Fig. 14. FL simulator block diagram. (a) Transmitting section. (b) Receiving section.

fading, are combined together with the thermal AWGN at the receiver input.

Simulations of the forward link were done either with the optional reference symbols included in the DPCCH for channel estimation or without them, this last option being more efficient in the presence of nonadaptive beams. The latter solution, which exploits the reference symbols on the primary CCPCH for channel estimation, not only allows one to save on-board power (by not transmitting unnecessary reference symbols in each carrier) but also reduces the interference level. Reference symbols are typically transmitted at a higher power level with respect to information data symbols causing a burst of higher interference power. Moreover, a better channel estimation is often possible by exploiting the CCPCH reference symbols instead of those embedded in the DPCCH because of the typically larger power of CCPCH. In the following results, we will assume that the DPCCH takes 20% of the overall time-slot length in case the optional reference symbols are transmitted. In that case, the DPCCH consists of one reference symbol and one TPC/TFCI symbol per slot. In the absence of the optional reference symbols, the DPCCH takes instead 10% of the time slot (only one TPC/TFCI symbol per slot is transmitted). Even when refer-

ence symbols are included in the DPCCH, we have assumed in our simulations that frequency tracking is anyway performed via the reference symbols included on the CCPCH (AFC bandwidth was 6 Hz). No case-by-case optimization of the reference symbol power level was done. If not stated otherwise, reference symbols are transmitted at a relative level (with respect to other symbols in the carrier) of $+6$ and $+4$ dB, respectively, for the primary CCPCH and the DPCCH while TPC/TFCI bits use the same level as the DPDCH. With this hypothesis, an overhead of 1.58 or 0.46 dB results due to the usage of the DPCCH, respectively, in the options with and without reference symbols.

For the FEC, the standard rate $r = 1/3$ or $1/2$, constraint length $k = 9$ convolutional codes have been adopted here. For data rates higher than 32 Kb/s, the adoption of turbo codes common to T-UMTS is currently envisaged [19]. Suitable bit puncturing or repetition is used to fit the encoded bitstream to the frame structure as detailed in [19]. Finally, channel interleaving over a 20-ms (half -chip-rate option) or 10-ms (full-chip-rate option) frame is assumed.

Results are typically given as a function of the ratio between the single path bit energy E_p and the thermal noise density N_o, where the bit energy per path E_p also includes the overhead due to the DPCCH. It must be stressed that N_0 only accounts for thermal noise and not for the MAI. Clearly, for the same E_p/N_o, the actual performance will strongly depend, in addition to the propagation channel conditions, also on the current MAI PSD level I_0. The MAI level used for deriving the simulation results here summarized can be deducted from the figures reporting the results themselves by considering how many spacecraft (S/C) are visible, how many equilevel beams of each S/C are received by the wanted user, and how many traffic channels are carried by each beam. For completeness, simulation results are also reported for the case of no CDMA MAI. These results are of general applicability for all cases whereby AWGN plus MAI can be assimilated to an equivalent AWGN Gausian process with PSD $N_0 + I_0$.

The simulations were performed assuming a floating-point implementation of the demodulator. As far as the relevant demodulator algorithms used in simulations, the following applies.

1) Chip tracking assumed a conventional noncoherent DLL with a loop bandwidth of approximately 10 Hz.
2) AFC was performed, during the steady-state phase, with a digital CPAFC [35] sampled once per time slot and operating on the SCH channel only. A loop bandwidth of about 6 Hz was assumed.
3) Channel estimation was also performed on the SCH by using a moving average filter of length equal to six slots.

A first set of simulations was aimed at verifying the performance of a conventional CR under the two fading scenarios previously discussed with and without satellite path diversity. A second set of simulations was aimed at verifying the potential gain coming from the adoption of the MOE interference mitigating receiver. Finally, the impact of on-board nonlinearity was assessed.

1) Conventional CR: Figs. 15 and 16 report the CR simulation results for 8-kbit/s channels in *fast* and *slow* fading for single and dual diversity. The basic code rate is $r = 1/3\,(k = 9)$; hence, assuming the use of an 8-bit CRC plus 8-bit tail at the end of each frame, 528 bits would be available at the output of the convolutional code. Some bit repetition is thus used to fill the frame (576 bits total available). No dedicated reference symbols are used. It shall be observed that the number of traffic carriers used in the simulation takes into account that with double diversity, the overall number of DPDCH/DPCCH to be transmitted shall double to maintain the same traffic level. Nevertheless, double diversity provides a consistent advantage (especially for the slow fading case) even when the total $E_b/N_o = E_p/N_0 + 3$ dB is considered in lieu of the *per finger* E_p/N_o. Hence it can be concluded that satellite diversity provides increased capacity (for typical fading scenarios) even disregarding the QoS improvement provided thanks to link blockage probability reduction.

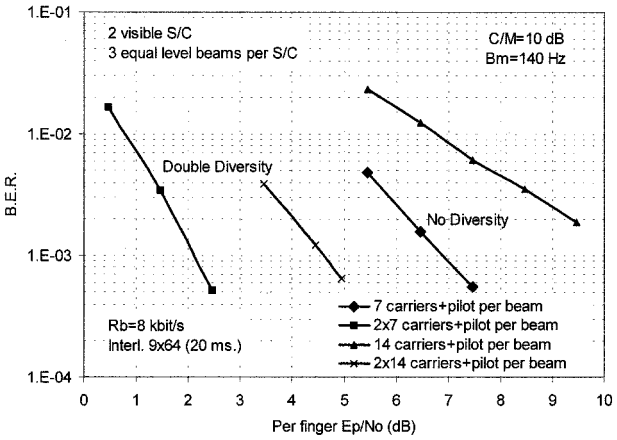

Fig. 15. Performance in single and double diversity with a conventional receiver. Fast fading case.

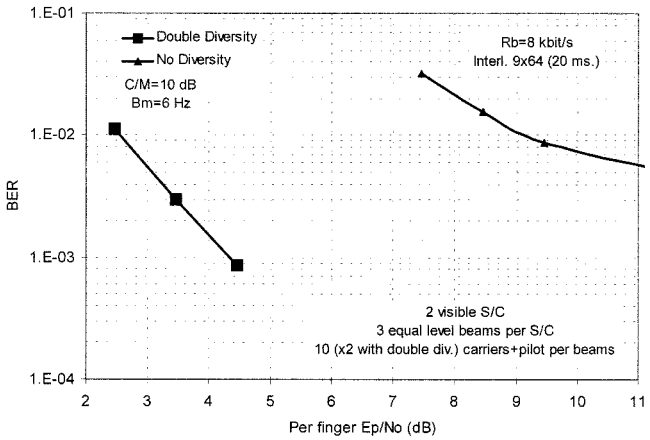

Fig. 16. Performance in single and double diversity with a conventional receiver. Slow fading case.

The peculiar nature of the FL CDMA interference has an impact on the way CDMA self-noise behaves. Fig.17 compares the simulated FL BER in the presence of the actual CDMA self-noise versus the equivalent $E_p/(N_0 + I_0)$ computed using the standard Gaussian approximation for the MAI for a scenario with slow fading and double diversity. This plot can be

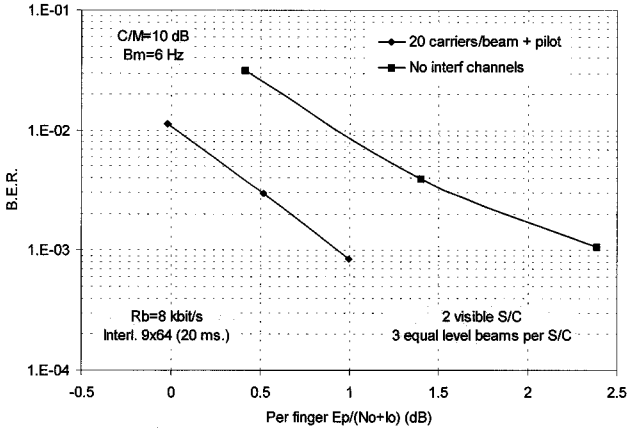

Fig. 17. Results with slow fading and double diversity versus the overall $E_b/(N_0 + I_0)$ in two different interference scenarios. Reference symbols are not included in the DPCCH.

compared with that obtained by replacing the background FL MAI with an equivalent white Gaussian noise generator. The realistic system simulation shows about 1.5 dB better performance than that predicted by the AWGN MAI model for the case of dual diversity with slow fading. Other simulations, also including reference symbols in the DPCCH, showed an even higher difference in performance (more than 2 dB). It follows that the FL CDMA interference cannot be assimilated to thermal noise in the presence of slow fading. This fact is explained by considering that for each satellite, channel fading affects in the same way the wanted and interfering channels. Hence, during fading, the instantaneous E_b/N_0 decreases while the E_b/I_0 due to the other satellite beams remains constant. Thus the overall $E_b/(N_0+I_0)$ fluctuation due to fading is mitigated. Simulation results for fast fading (not included here) show that in this case, the AWGN MAI model is adequate.

Table III shows the required $E_b/(N_0 + I_0)$ to achieve a $\mathrm{FER} = 10^{-2}$ or $\mathrm{BER} = 10^{-3}$ for the case of two different Ricean fading channels with a user bit rate of 8-kbit/s channel with an AWGN MAI model and full-rate spreading option (3.84 Mchip/s).

2) Blind MOE Receiver Performance: As previously mentioned, the linear blind MOE receiver with LMS adaptation was selected for possible use on the FL. Although theoretical and simulation results on blind-MOE receiver performance also including some static channel estimation error were already available in the literature [14], none was representative of a heavily coded multirate CDMA rake adaptive demodulator exploiting path diversity. It is in fact known that demodulator operations at low SNR due to the powerful FEC scheme selected are in favor of the CR. The following performance of the blind-MOE receiver have been obtained in a realistic FL multibeam multisatellite scenario, taking into account also the peculiarities of the access scheme and the effect of nonideal signal parameter estimation. One of the main deviations from reality is represented by the lack of power-control-level adjustment of the different forward-link channels. This issue has been rigorously tackled in [16].

A short randomization code (256 chips) was employed. It shall be observed that the selected randomization code period is still longer than the data symbol (at least for bit rate exceeding 4.8 Kbit/s). The blind-MOE receiver in this case has to be implemented as a set of independent receivers, each working on a different subinterval of the randomization code period. It can be found that the adaptation speed of the algorithm is almost independent of the data rate.

Some interesting causes of performance degradation have been discovered. One of the peculiarities of the proposed access scheme is the nonconstant envelope of the traffic channel, particularly when reference symbols are embedded in the DPCCH associated to each DPDCH. The presence of this amplitude variation makes the performance of the blind MOE somewhat suboptimum compared to that achievable with constant envelope. It was also found that fixed reference symbols, or other possible repetitive patterns, lead to a correlation between interference and wanted carrier that may occasionally strongly degrade the MOE receiver performance. Consequently, if reference symbols cannot be avoided, a scrambler to randomize carrier data (including reference symbols in the DPCCH associated to each DPDCH) is mandatory for compatibility with the use of the blind-MOE technique.

An additional degradation comes from the DLL tracking error. In addition to the DLL timing jitter, a bias in the recovered timing is inherent in the use of short spreading codes [24] as required by the adoption of blind-MOE adaptive detectors. The bias is typically more pronounced in the FL than in the RL due to the chip synchronization between different channels belonging to the same satellite. Moreover, it is typically worse in a scenario were the number of intrabeam carriers is larger with respect to the total number of carriers received by the terminal. At the practical demodulator SNR operating point, this DLL bias was found, however, to have only a negligible impact on the blind-MOE BER performance. Finally, the presence of intrabeam orthogonal interference contributes to impairing the effectiveness of blind-MOE interference mitigation, as it does not affect the CR but only the blind MOE by stealing signal space dimensionalities.

Fig. 18 shows a set of simulation results with and without MOE in a double-diversity fading channel. It appears that, notwithstanding all the above-mentioned factors contributing to degrading the effectiveness of the blind-MOE receiver, its potential in reducing the negative effects of carrier unbalance is quite evident. It should be emphasized that in the forward link of a power-controlled multibeam channel, power unbalance is a typical operating condition, as users situated at the beam edge will experience higher interference than those located inside the beam. For situations with uniform carrier level, the advantages of interference mitigation are not very significant due to the strong FEC coding, which actually makes the operational SNIR, after despreading, very small (even less than 0 dB). At this low SNIR, thermal noise is typically dominating. Finally, it shall be observed that the overall number of carriers in the example of Fig. 18 is slightly larger than the spreading factor; hence the system is working in the so-called dimensional clash zone, i.e., the number of interferers exceeds the CDMA signal space dimensionality.

3) Nonlinearity Effects: During initial modulation/spreading format tradeoff, the impact of the satellite

TABLE III
PER PATH $E_b/(N_0 + I_0)$ REQUIRED FOR BER $= 10^{-3}$, FER $= 10^{-2}$, AND AN 8-kbit/s CHANNEL (FORWARD LINK). A FRAME IS 10 ms. CHIP RATE IS 3.84 Mchip/s AND INTERLEAVER IS ONE FRAME LONG. CONVOLUTIONAL CODING ($k = 9, r = 1/3$)

Ricean Channel Characteristics			$[E_b/(N_0+I_0)]_{req}$ (dB)	
Diversity order	*C/M* (dB)	Fading bandwidth Bm (Hz)	$BER=10^{-3}$	$FER=10^{-2}$
1	10	6	8.1	7.4
1	10	140	5.2	5
2	10	6	3.0	2.4
2	10	140	1.4	1.5
1	15	6	4.7	4.5
1	15	140	3.75	3.75
2	15	6	1.0	0.8
2	15	140	0.5	0.6

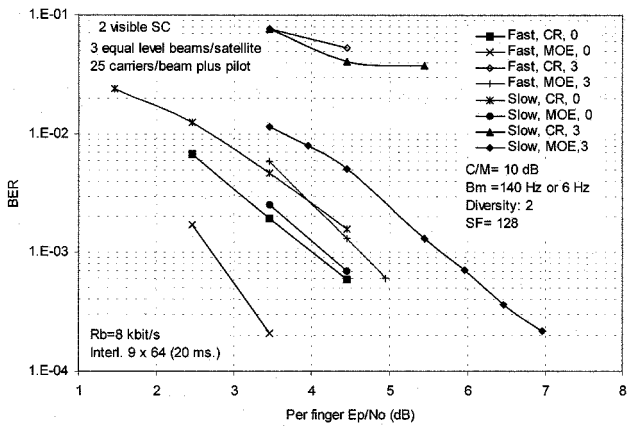

Fig. 18. BER performance with MOE in a double satellite diversity. The wanted user receives three beams per satellite at the same level. Each beam (including wanted) carries 25 carriers plus the pilot. Interfering carriers are either at 0 or +3 dB level with respect to wanted carriers. Reference symbols only on PCCPCH (+6 dB level with respect to other symbols). Blind-MOE algorithm window size = 2 symbol.

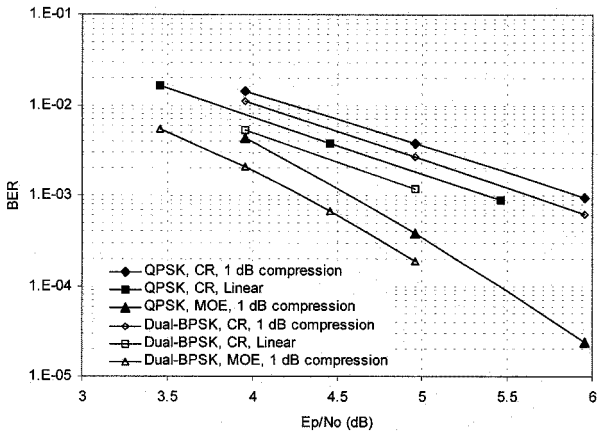

Fig. 19. Nonlinearity effects on performance. The simulated case correspond to an AWGN channel with 12 synchronous interfering carriers and 40 asynchronous interfering carriers, all having the same level as the wanted carrier.

nonlinearity was considered. Assuming the worst case single SSPA for the payload nonlinearity [23] (see Fig. 14), it was found that QPSK modulation is more sensitive to nonlinearity than dual BPSK. However, dual BPSK also requires double the number of spreading codes and is potentially performing less in conjunction with interference mitigation techniques. The greater sensitivity of QPSK to nonlinear distortion was actually verified when the optional reference symbols were included in the traffic channels. Without the higher level optional reference symbols included in the traffic channels, the effect of nonlinearity was milder (see Fig. 19). In this case, the performance difference between the two modulation/spreading formats is due to the lower sensitivity of dual BPSK to carrier phase and frequency error more than to the lower sensitivity to nonlinearity. Note that the MOE detector gain versus the CR amounts to about 1.5 dB due to its capability to mitigate the loss of code orthogonality effects.

B. Reverse-Link Physical-Layer Performance

The RL simulator block diagram is shown in Fig. 20. The wanted signal is actually fed in parallel to multiple satellite paths, each one experiencing independent fading and a different delay. Differently from FL, all active mobile users will experience an independent fading process [hence independent fading is generated for each interferer in Fig. 20(b)]. Moreover, no orthogonal CDMA interference occurs. Note that for RL simulations, the impact of TCFI frame rate detection errors have not been considered.

As discussed previously, the RL of SW-CDMA can greatly benefit from satellite diversity. This is confirmed in Fig. 21, which refers to a fast fading channel. For a slow fading channel, the advantage of diversity would have been even more significant.

In the presence of diversity, the SNR per rake finger can be significantly reduced, thus lowering the potential advantages of using linear interference mitigation techniques. Fig. 22 shows some examples of the RL performance, with and without MOE in presence of real CDMA MAI. As expected, MOE is advantageous when near–far effects are more significant, but power control will make their occurrence less likely.

Finally, Table IV shows the required $E_b/(N_0+I_0)$ to achieve an FER $= 10^{-2}$ and for a BER $= 10^{-3}$ for the case of an 8-kbit/s channel assuming an AWGN MAI model and full-rate spreading option (3.84 Mchip/s).

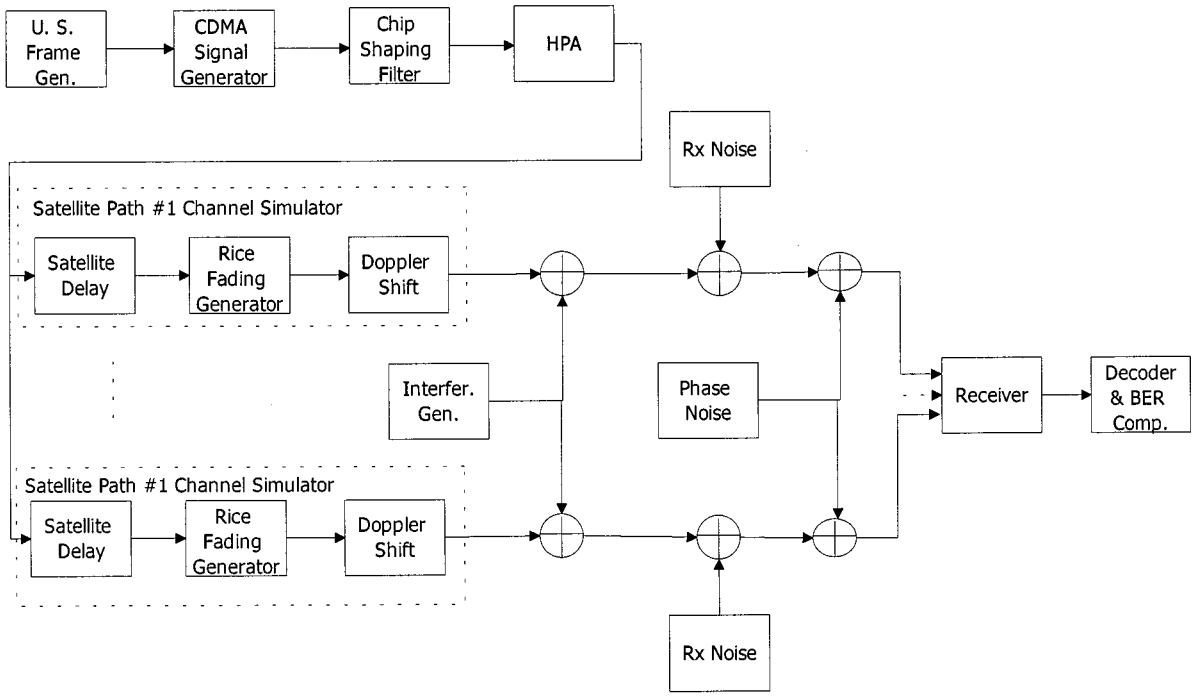

(a)

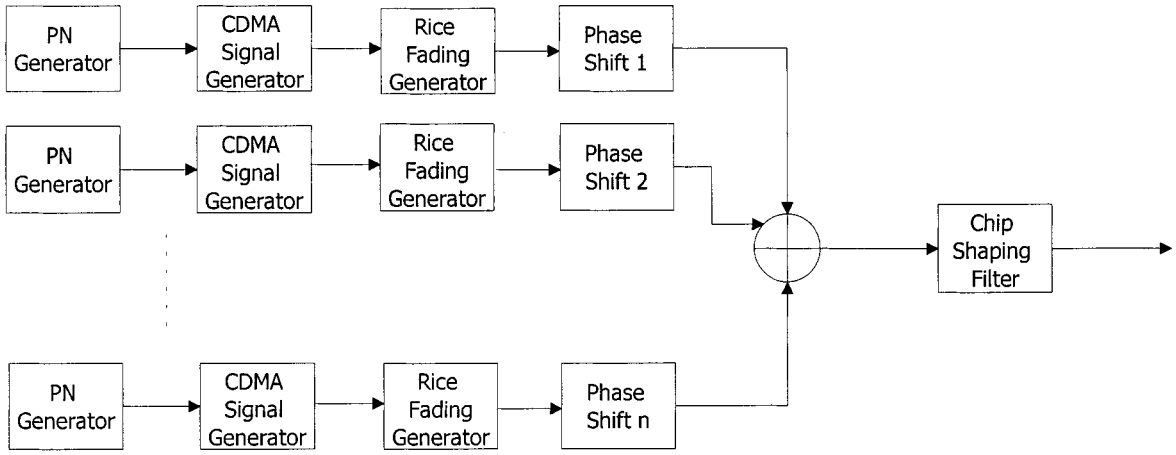

(b)

Fig. 20. Reverse-link simulator architecture. (a) Top level architecture. (b) Interference generation.

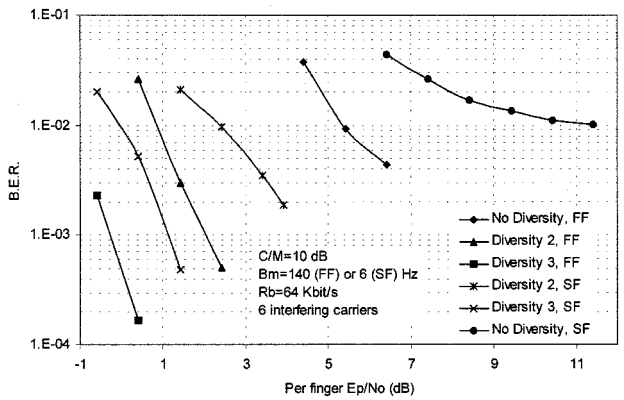

Fig. 21. FF and SF RL BER with diversity 1, 2, 3 and CR detector. Interfering carriers have the same level as the wanted one. The DPCCH power is 10% of that of the DPDCH. The basic FEC coding is $r = 1/2$.

Regarding the demodulator algorithms adopted in the simulations, the following applies.

1) Chip tracking assumed a conventional noncoherent DLL with a loop bandwidth of approximately 10 Hz only acting on the DPCCH.
2) AFC was performed with a digital CPAFC [35] operating on the reference symbols included on the DPCCH channel. The loop sampling period (in the steady-state phase) was one slot. A loop bandwidth of about 6 Hz was assumed.
3) Channel estimation was also performed on the reference symbols of the DPCCH by using a moving average filter of length equal to six slots.

1) Nonlinearity Effects: As described previously, the SW-CDMA RL DPCCH signaling channel is multiplexed by exploiting carrier phase and code orthogonality in order

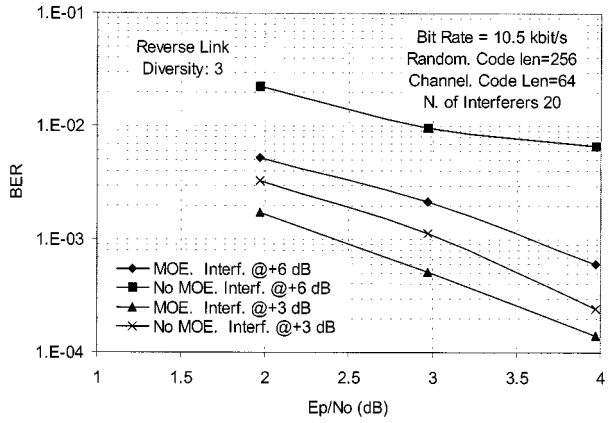

Fig. 22. RL BER with and without blind-MOE detector. The number of interfering channels was 20 with relative level with respect to the wanted carrier of 3 or 6 dB.

to minimize DPDCH crosstalk. This channel multiplexing technique greatly reduces envelope fluctuations [7], which represent a major drawback for a satellite terminal because the high-power amplifier must operate in its nonlinear region in order to maximize the transmitted power and DC/RF efficiency and to ensure a longer battery duration. The advantages of this quadrature DPCCH insertion compared to the in-phase option have been verified by evaluating the impact on the transmitted signal spectrum after MES nonlinear amplification. This has been simulated using a typical solid-state amplifier. The simulated SSPA output spectrum, for a DPCCH/DPDCH power ratio equal to -6 dB (corresponding to the worst case 2.4-Kbit/s bit rate) and for an SSPA drive corresponding to the 1-dB compression point, is shown in Fig. 23. The lower (dashed) power spectral density corresponds to the quadrature CDMP scheme. When compared with the power spectral density obtained without pilot insertion, the results are very close (being very close to the pilot-free power spectral density plot, it has not been included in the plot to preserve graph readability), meaning that the proposed pilot insertion technique suppresses sidelobe regrowth very efficiently. More specifically, Fig. 23 shows that the in-phase pilot multiplexing is characterized by an out-of-band power that is 5 dB higher than that of the selected pilot insertion scheme, which significantly increases adjacent channel interference.

C. Source Coding Simulations

Here we present the performance obtained by joining the proposed physical layer with audio and video telephony services. Two scenarios for digital speech coding are investigated. High-quality voice is considered by using the ITU-T G.729 standard at 8 kbits/s [24]. This standard produces toll-quality speech with an algorithmic delay of only 15 ms [27]. The use of a lower quality and lower delay speech coding standard, the ITU-T G.723.1 at 6.3 kbits/s, is also simulated [28]. With both of these cases, a silence compression scheme is used to lower the bit rate during silence segments. The video telephone uses the ITU-T H.324 [29] multimedia standard to combine the G.723.1 speech at 6.3 kbits/s and the ITU-T H.263 video at 51.2 kbits/s [30], at an overall rate of 64 kbits/s. The video telephone image format is QCIF (144 lines $\times$ 176 pixels), updated at 10 frames/s, and Annexes D, F, J, S, and T are used in the coder [30].

The specific channel coding design is performed by assuming two channel coding levels. It is assumed that the inner channel convolutional decoding level (Viterbi decoder) performs hard decisions and provides the audio and video services with a bit error rate of 10^{-3}. To better protect the different source coding schemes, an outer channel coding level specific to each standard is used. The choice of this second coding level is done by carefully studying the effects of the channel errors on the source decoder quality and by establishing specific unequal error protection levels. The results of this study appear in [25]. In both the G.729- and the G.723.1-based telephony services, BCH codes are selected as outer codes [25]. These choices produce a maximum coded bit rate of 10.2 kbits/s in the G.729 case and 8.07 kbits/s for the G.723.1-based service. The results of the sensitivity analysis performed on the H.263 video standard have indicated that a good strategy is to protect all the coded bits evenly, at an error rate of 10^{-5} or better. An 8-bit (255 223) Reed–Solomon code is selected to protect all the multiplexed bits (audio, video, and overhead). Video error propagation is also reduced by forcing every 16×16 pixels macroblock to be coded by transform coding, at least once every 20 frames. The video-telephony coded bit rate is 73.18 kbits/s. To combat the effects of the error bursts introduced by the inner Viterbi decoder and the fading channel, specific interleavers were designed for the different types of services and outer coding schemes [25].

The simulated performance of the different source coding scenarios has been evaluated by using a combination of objective and subjective measurements. The BER at the output of the outer decoder has been measured to give an indication of the interleaver efficiency. In the case of the speech services, the segmental SNR (SEGSNR) has been computed and subjective listening evaluations have been conducted. For the video-telephony service, a subjective evaluation has been performed. The full results appeared in [25]. Partial results are presented below. A nonfrequency-selective Ricean fading channel is simulated, with a Ricean factor of 10 dB. As indicated before, fast fading refers to a vehicle speed of 70 Km/h and corresponds to a Doppler spread of 140 Hz. Slow fading corresponds to a speed of 3 Km/h and a Doppler spread of 6 Hz. All the simulations are run using the FL channel scenario.

1) G.729 Speech Telephony: The received voice quality has been evaluated when the system is operating at threshold, i.e., when the inner Viterbi decoder delivers an average BER of around 10^{-3}. The results for a 1-min audio passage are given in Table V. It is noted that the SEGSNR is always close to its largest possible value of 1.5. The degradation in voice quality, as evaluated subjectively (in informal tests), is also indicated in this table. This degradation is always small and is dominated by the burst of errors still present in the slowest fading cases. Between these error bursts, the subjective quality is high. The speech intelligibility is high at all times.

2) G.723.1 Speech Telephony: In this case, because of the limitations in the overall processing delay, the outer interleaving is limited to one voice frame. The results on voice quality, for an operation at threshold (channel BER at 10^{-3}), are given in Table VI. Note that despite the fact that the BER performance

TABLE IV
PER PATH $E_b/(N_0 + I_0)$ REQUIRED FOR BER $= 10^{-3}$ AND FER $= 10^{-2}$ AND AN 8-kbit/s CHANNEL (REVERSE LINK). A FRAME IS 10-ms PERIOD; CHIP RATE IS 3.84 Mchip/s AND INTERLEAVER IS ONE FRAME LONG. CONVOLUTIONAL CODING ($k = 9, r = 1/3$)

Ricean Channel Characteristics			***[E_b/(N_0+I_0)]$_{req}$ (dB)***	
Diversity order	*C/M* (dB)	Fading bandwidth Bm (Hz)	*BER=10^{-3}*	*FER=10^{-2}*
1	10	6	9.5	8
1	10	140	6	5.7
3	10	6	1.25	1.35
3	10	140	0.5	0.5
1	15	6	5.5	5.3
1	15	140	4.5	4.45
3	15	6	0.35	0.35
3	15	140	0.1	0.2

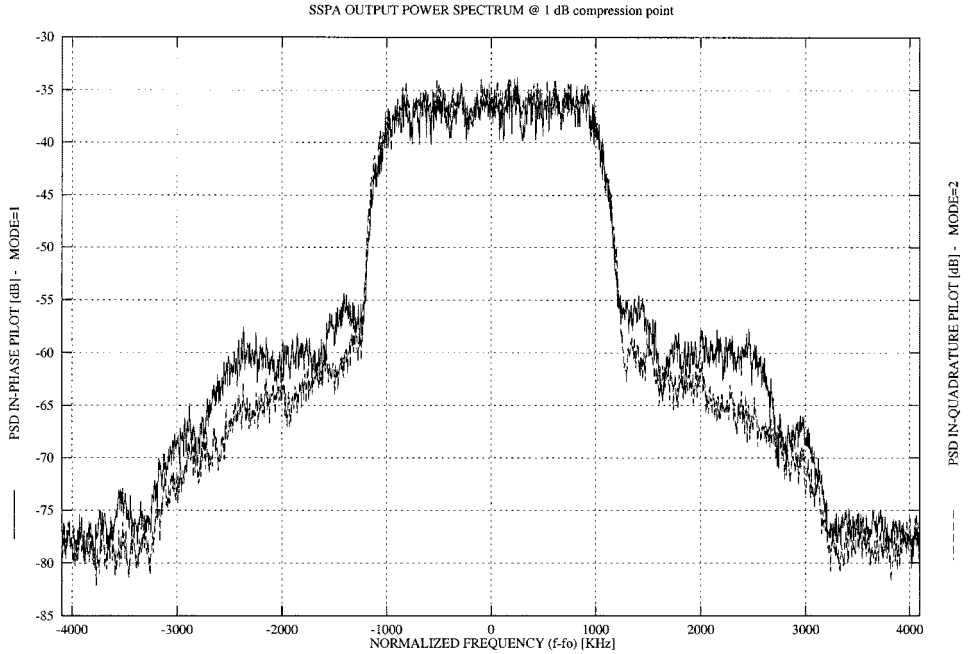

Fig. 23. Simulated transmitted signal power flux density for DPCCH/DPDCH power ratio equal to -6 dB [2.4 Kb/s], MES SSPA at 1-dB compression point: (a) continuous line: in-phase DPCCH; (b) dash-dotted line: SW-CDMA with quadrature DPCCH.

is similar to that encountered in the G.729 scenario, the voice degradation is always high, and the speech intelligibility is deteriorated. This tends to favor the use of the G.729 standard over that of the G.723.1 standard on a bursty channel.

3) Video Telephony: The video telephony service was evaluated for 1-min sequences. The BER measured at the output of the (255, 223) Reed–Solomon decoder is indicated in Table VII. These results are better than the BER subjective threshold of 10^{-5} for the AWGN and the fast fading channel but are poor for the slow fading cases. They indicate that the combination of the outer code and the outer interleaver is not powerful enough to deal with the error burst distribution typical of the slow S-UMTS channel. The subjective degradation corresponding to the cases of Table VII is indicated in Table VIII. As expected, the subjective quality is degraded in the slowest fading cases. This is particularly true for the video portion of the communications, in which even the smallest artifact is annoying. The reproduction of the audio sequence could benefit from using the G.729 standard instead of the G.723.1, although this would not comply with the H.324 multimedia standard.

The simulation results of this section show that speech telephony is possible with good quality, over all the channel scenarios at a coded bit rate of 10.2 kbits/s, by using the ITU G.729 standard. The design based on the G.723.1 standard, and operating at a coded bit rate of 8.07 kbits/s, is not satisfactory. To increase the quality of this latter design, either more channel resources are required, to increase the channel coding redundancy, or more delay needs to be incorporated in the system, to increase the interleaver length. Despite a powerful outer coding scheme and a long outer interleaver, the quality of the videotelephony service is acceptable only in the AWGN and the fast fading cases. Extending the operation to the slow fading scenarios would require some combination of satellite diversity, lower rate channel coding, and error concealment in the video

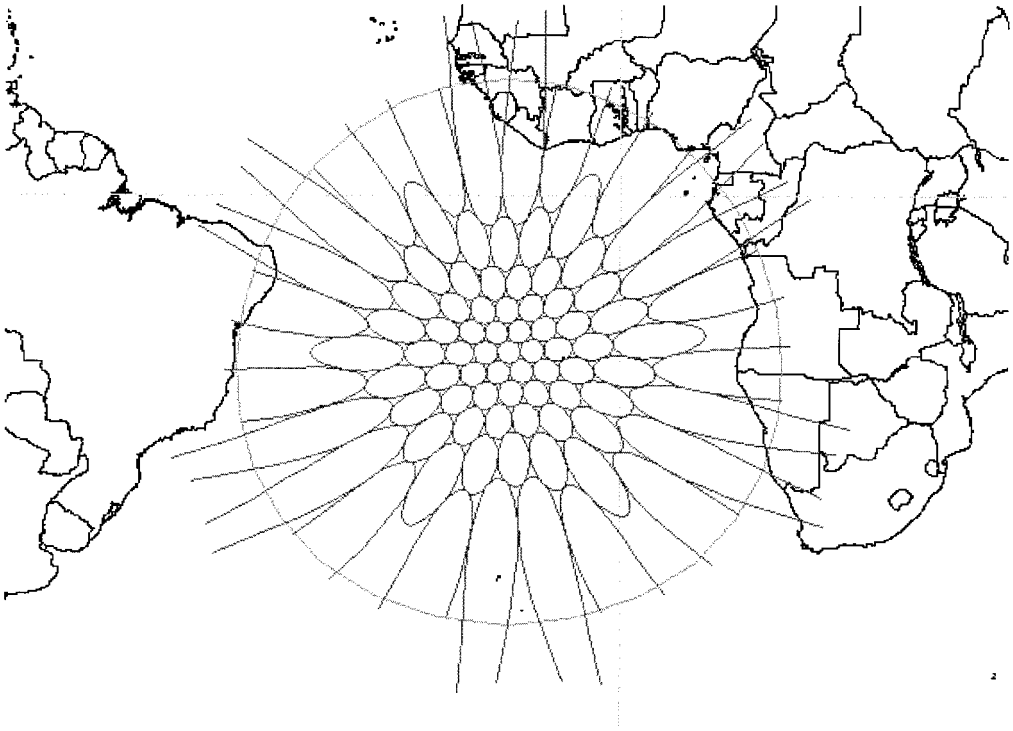

Fig. 24. LEO beam footprint.

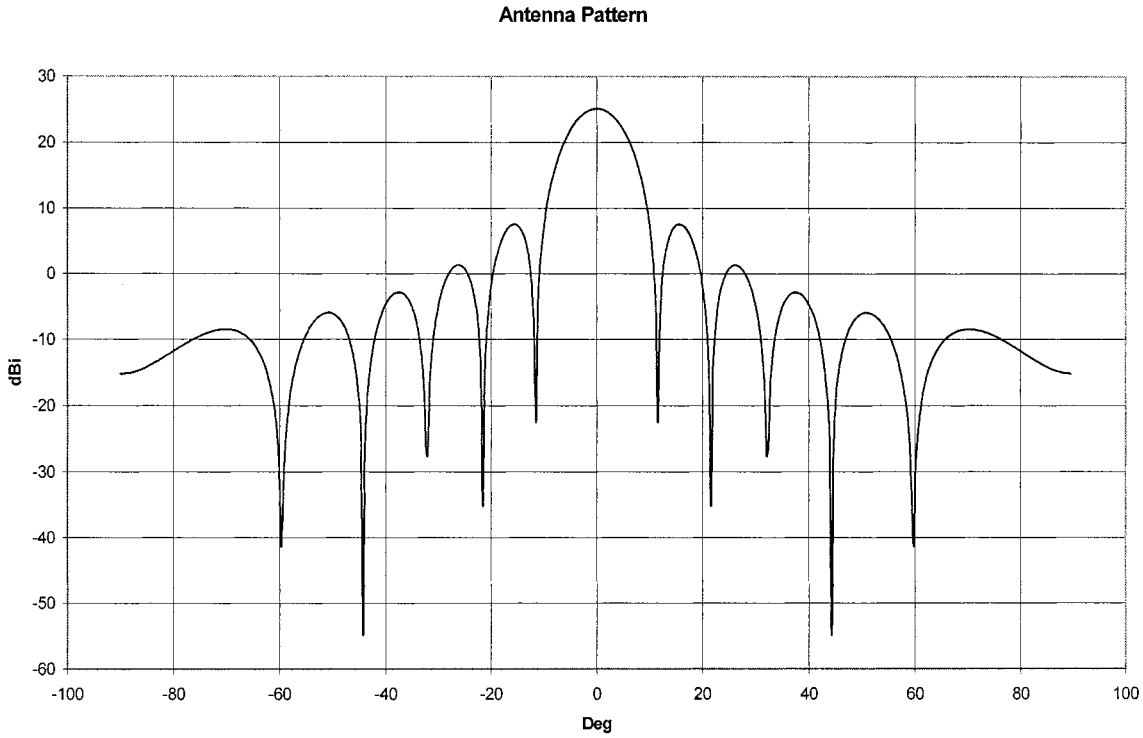

Fig. 25. LEO antenna pattern.

decoder. Note that double satellite diversity allows a significant drop in E_b/N_0 for similar BERs but that the detrimental effect of the error bursts is not significantly reduced.

V. System Capacity Study Case

To better clarify the kind of capacity performance achievable by the proposed RTT, a set of study case results are provided. System capacity has been derived with two different methodologies.

I) By performing a brute-force Monte Carlo analysis of a constellation of multibeam satellites assuming that users are distributed over a uniformly spaced gird of points. Initially to each grid point an arbitrary traffic load can be assigned based on the expected traffic dis-

TABLE V
G.729 OBJECTIVE VOICE QUALITY (SEGSNR) AND THE SUBJECTIVE DEGRADATION FOR A CHANNEL BER of 10^{-3}. THE ERROR-FREE SEGSNR IS 1.5 dB. THE DEGRADATION SCALE IS: NONE, SMALL, MEDIUM, AND HIGH

Channel	Eb/No (dB)	SEGSNR (dB)	Subjective Degradation	Intelligibility
AWGN	4	1.41	small	high
Fast fading (140 Hz)	6	1.42	small	high
Slow fading (6 Hz)	9	1.44	small	high
Slow fading with double satellite diversity	4	1.45	small	high

TABLE VI
G.723.1 OBJECTIVE VOICE QUALITY (SEGSNR) AND THE SUBJECTIVE DEGRADATION FOR A CHANNEL BER OF 10^{3}. THE ERROR-FREE SEGSNR IS 10.97 dB. THE DEGRADATION SCALE IS: NONE, SMALL, MEDIUM, AND HIGH

Channel	Eb/No (dB)	SEGSNR (dB)	Subjective Degr.	Intelligibility
AWGN	3.5	9.16	high	medium
Fast fading (140 Hz)	5.75	10.18	high	medium
Slow fading (6 Hz)	8.5	10.38	high	medium
Slow fading with double satellite diversity	4	10.5	high	medium

TABLE VII
THE MEASURED BER AT THE OUTPUT OF THE (255, 223) REED–SOLOMON DECODER IN THE VIDEO-TELEPHONY SERVICE FOR A CHANNEL BER OF 10^{-3}

Channel	Eb/No (dB)	Outer BER on R-S Decoded Bits
AWGN	3	$< 1x10^{-10}$
Fast fading (140 Hz)	4.5	$< 1x10^{-10}$
Slow fading (6 Hz)	8	$8x10^{-4}$
Slow fading with double satellite diversity	4	$4x10^{-4}$

TABLE VIII
THE SUBJECTIVE DEGRADATION FOR THE CASES OF TABLE VII. THE DEGRADATION SCALE IS: NONE, SMALL, MEDIUM, AND HIGH

Channel	*Audio* Subjective Degradation	*Video* Subjective Degradation
AWGN	none	none
Fast fading (140 Hz)	none	none
Slow fading (6 Hz)	high	high
Slow fading with double satellite diversity	high	high

tribution. For each simulation time step, active users are allocated to satellites and beams in view according to the BCCH signal strength reports provided by each user terminal and selected maximum diversity order. Power assigned to each user location both in the forward and reverse link is adjusted through a power-control loop until all locations achieve the required SNIR as derived from physical-layer simulations. In case no global convergence is achieved, the number of user locations experiencing outage is recorded. Also possible satellite or user terminal RF power limit violation can be recorded or taken into account for outage calculation. Blockage is accounted for when no Walsh channelization codes are available for new physical channels. Then the constellation geometry is modified according to the selected time step and the procedure repeated. In this way, the simulation allowsone to assess the current system outage probability for a given capacity. In this way, it is also possible to compute the average/peak satellite and user terminal power required to support the current user population and traffic distribution. Although accurate (exact satellite antenna beam patterns are simulated jointly with power-control effects and real traffic distribution), this approach is highly time consuming.

II) By performing a simplified one-dimensional link budget analysis that takes into account the statistical satellite antenna parameters and the other system pa-

TABLE IX
SYSTEM PARAMETERS

Constellation type	Walker
Number of orbital planes	8
Number of satellite in each orbital plane	6
Semi Major Axis	7792 Km
Inclination (degrees)	52
Number of satellite beams	85
Minimum elevation angle for visibility of serving satellite	10 degrees
Satellite average antenna gain	21.3 dB
Satellite peak antenna gain (inner/outer)	25.8 / 24.0 dBi
Satellite NPR	> 16 dB
Satellite maximum RF power	500 W
Satellite transmit antenna average [I/C]	-2 dB
Satellite receive noise temperature	500 K
Hand-held maximum EIRP	-4 dBW
Hand-held user terminal average G/T	-26 dB/K

TABLE X
PHYSICAL-LAYER PARAMETERS

Multiple access scheme	CDMA/FDMA
Number of frequency slots	2
Chip rate	3.84 Mchip/s
Up-link frequency	2.000 GHz
Down-link frequency	2.190 GHz
Full bandwidth	10 MHz
Data rate	8 Kbit/s
Traffic activity factor	0.4
Doppler spread: slow fading	6 Hz
Rician fading; channel C/M	10 dB
Maximum forward link satellite diversity order	2
Maximum reverse link satellite diversity order	3
Power control error	0.25 dB

rameters in the way described in [16]. This approach, though much simpler, is quite accurate only for the average analysis and requires uniform traffic assumptions. The main purpose of this approach has been to validate the full-blown simulator and to provide an easy way to perform initial system parameter optimization. More details of this very useful simplified approach are reported in [16].

The system evaluation has been done with reference to a LEO constellation whose characteristics are summarized in Table IX, Fig. 24, and Fig. 25 for the satellite antenna pattern, and to the physical-layer parameters of Table X. Note that we took the worst case of a slow fading Ricean channel with $C/M = 10$ dB. Main simulation results are summarized in Table XI. Those dynamic constellation simulation results in terms of average capacity have been successfully compared with the simplified approach described in [16]. It appears that the use of a highly efficient RTT jointly with advanced satellite antenna design allows for achieving an high capacity system. Note that due to the reverse-link path diversity exploitation, the system is typically forward-link capacity limited. Further capacity increase not accounted for in Table XI can be achieved by implementing more advanced interference mitigating detectors. The lack of traffic over nondry Earth regions reduces the LEO capacity by a factor of three.

VI. CONCLUSION

In this paper, we presented the main results of an ESA-sponsored investigation about a third-generation air interface, identified as SW-CDMA, proposed for the satellite component of IMT 2000. The proposed air interface approved as part of the ITU IMT-2000 family and by ETSI as an S-UMTS voluntary radio interface specification [36] has been devised by minimizing the differences with respect to the UMTS UTRA W-CDMA air interface. The air interface adaptations required for the satellite environment are mainly residing in the power-control algorithm and updating rate, and relate framing specification impact. Optimized four-level power control allows one to effectively counteract typical satellite signal power variation dynamic but not the mild Rician fading. A simplified procedure for the initial mobile terminal code acquisition has been devised and analyzed. The coding, modulation, and spreading approach closely follows the terrestrial counterpart

TABLE XI
CAPACITY SIMULATION RESULTS

Parameter	Uniform user population	Dry lands only users
Number of active channels forward link	517272	172448
Average FWD capacity per satellite (channels)	10776	3593
Average FWD capacity per beam and frequency slot (channels)	63.4	21.13
Average satellite RF power consumed (W)	296	98
Peak satellite RF power consumed (W)	516	538
Forward link outage probability (%)	0.1	0.1
Number of active channels reverse link	901252	270000
Average RTN capacity per satellite (channels)	18776	5625
Average RTN capacity per beam and frequency slot (channels)	110.4	33.1
Average terminal EIRP (dBW)	0.14	0.12
Reverse link outage probability (%)	1.0	0.8

except for the optional short scrambling sequence in the forward link that allows the exploitation of simplified CDMA multiuser detector in the mobile terminal. The physical-layer performance including channel estimation showed good performance over a variety of channel conditions and demonstrated the great gain provided by satellite path diversity for both the forward and the reverse link. The optional MUD allows improved performance in the forward link, removing a considerable part of the other interfering beams and the cochannel interference due to the loss of CDM orthogonality due to the satellite nonlinearity. Physical-layer results have been complemented by end-to-end simulation including the audio/video source codec showing the relation among operation SNIR, BER, and quality of service. An in-depth capacity investigation for a third-generation possible LEO constellation has also been reported, showing the remarkable RTT capacity capabilities.

Summarizing, it has been shown that with a limited number of adaptations, the satellite UMTS component can benefit from the ongoing terrestrial UMTS standardization and development effort. In this framework, ESA is actively supporting the development and demonstration of an open S-UMTS air interface maximizing the commonality with the emerging T-UMTS standard. It is felt that this approach may eventually lead to a successful and truly complementary S-UMTS component development. Further work is required to optimize the radio resource algorithms and the medium-access control jointly with the physical layer for effective packet data service provision.

REFERENCES

[1] *Detailed Specifications of the Radio Interfaces of IMT-2000*, Nov. 1999.

[2] B. Lyons, B. Mazur, J. Lodge, M. Moher, S. Crozier, and L. Erup, "A high capacity third-generation mobile satellite system design," *Eur. Trans. Telecommun.*, vol. 9, July/Aug. 1998.

[3] *Robust Modulation and Coding for Personal Communication Systems*.

[4] E. Lutz, D. Cygan, M. Dippold, F. Dolainsky, and W. Papke, "The land mobile satellite channel—Recording, statistics and channel model," *IEEE Trans. Veh. Technol.*, vol. 40, pp. 375–386, May 1991.

[5] Y. Karasawa *et al.*, "Analysis of availability improvement in LMSS by means of satellite diversity based on three-state propagation channel model," *IEEE Trans. Veh. Technol.*, vol. 46, pp. 1047–1056, Nov. 1997.

[6] G. E. Corazza and C. Caini, "Satellite diversity exploitation in mobile satellite CDMA systems," in *IEEE Wireless Communication and Networking Conf. (WCNC'99)*, New Orleans, LA, Sept. 21–24, 1999, pp. 1203–1207.

[7] G. E. Corazza and R. De Gaudenzi, "Pilot-aided coherent uplink for DS-CDMA satellite networks," *IEEE Trans. Commun.*, vol. 48, pp. 773–783, May 1999.

[8] G. E. Corazza, "On the MAX/TC criterion for code acquisition and its application to DS-SSMA systems," *IEEE Trans. Commun.*, vol. 44, pp. 1173–1182, Sept. 1996.

[9] M. K. Sust *et al.*, "Rapid acquisition concept for voice activated CDMA communication," in *Proc. IEEE Globecom 1990*, San Diego, CA.

[10] G. E. Corazza and A. V. Coralli, "Burst vs. continuous pilot acquisition in wideband CDMA cellular mobile systems," in *Proc. IEEE Wireless Communications and Networking Conf. (WNCN'99)*, New Orleans, LA, Sept. 21–24, 1999.

[11] R. De Gaudenzi, F. Giannetti, and M. Luise, "Signal recognition and signature code acquisition in CDMA mobile packet communications," *IEEE Trans. Veh. Technol.*, vol. 47, pp. 196–208, Feb. 1998.

[12] M. Honig, U. Madhow, and S. Verdu', "Blind adaptive multiuser detection," *IEEE Trans. Inform. Theory*, vol. 41, pp. 379–384, July 1995.

[13] U. Madhow, "Blind adaptive interference suppression for direct-sequence CDMA," *Proc. IEEE*, vol. 86, pp. 2049–2069, Oct. 1998.

[14] R. De Gaudenzi, J. Romero-Garcia, F. Giannetti, and M. Luise, "A frequency error resistant blind interference mitigating CDMA detector," *IEEE Trans. Commun.*, vol. 48, pp. 1070–1076, July 2000.

[15] *Multi User Interference Cancellation Demodulator*. Centro TEAM and SGS-Thomson Microelectronics, ESA Contract 13095/98/NL/SB.

[16] J. Romero-Garcia and R. De Gaudenzi, "On antenna design and capacity analysis for the FL of a multi-beam power controlled satellite CDMA network," *IEEE J. Select. Areas Commun.*, vol. 18, no. 7, pp. 1230–1244, 1999.

[17] *Technical Specification Group Radio Access Network*, 1999. 3rd Generation Partnership Project (3GPP), Release.

[18] *Technical Specification Group Radio Access Network—Physical Channel and Mapping of Transport Channels onto Physical Channels (FDD)*, 1999. 3rd Generation Partnership Project (3GPP), Release, Doc. 75-25-211.

[19] *Technical Specification Group Radio Access Network—Multiplexing and Channel Coding (FDD)*, 1999. 3rd Generation Partnership Project (3GPP), Release, Doc. 75-25-212.

[20] *Technical Specification Group Radio Access Network—Spreading and Modulation (FDD)*, 1999. 3rd Generation Partnership Project (3GPP), Release, Doc. 75-25-213.

[21] *Technical Specification Group Radio Access Network—Physical Layer Procedures (FDD)*, 1999. 3rd Generation Partnership Project (3GPP), Release, Doc. 75-25-214.

[22] F. Adachi *et al.*, "Tree structured generation of orthogonal spreading codes with different lengths for the FL of DS-CDMA," *Electron. Lett.*, vol. 33, no. 1, pp. 27–28, 1997.

[23] R. De Gaudenzi, "Globalstar paylaod nonlinearity effects on the FL CDMA multiplex: Part I; physical layer analysis," *IEEE Trans. Veh. Technol.*, pp. 960–976, May 1999.

[24] W. R. Braun, "PN acquisition and tracking performance in DS/CDMA systems with symbol length spreading sequences," *IEEE Trans. Commun.*, vol. 45, pp. 1595–1601, Dec. 1997.
[25] D. Boudreau, R. Lyons, G. Gallinaro, and R. De Gaudenzi, "A simulation of audio and video telephony services in a satellite UMTS environment," *Proc. Int. Mobile Satellite Communication Conf.'99*, June 1999.
[26] *Coding of Speech at 8 kbit/s using Conjugate-Structure Algebraic-Code-Excited Linear Prediction (CS-ACELP)*, Mar. 1996.
[27] R. V. Cox, "Three new speech coders from the ITU cover a range of applications," *IEEE Commun. Mag.*, vol. 35, pp. 40–47, Sept. 1997.
[28] *Dual Rate Speech Coder for Multimedia Communications Transmitting at 5.3 and 6.3 kbit/s*, Mar. 1996.
[29] *Terminal for Low Bit-Rate Multimedia Communication*, Feb. 1998.
[30] *Video Coding for Low Bitrate Communication*, Feb. 1998.
[31] R. De Gaudenzi, C. Elia, and R. Viola, "Band-limited quasisynchronounous CDMA: A novel multiple access technique for personal communication satellite systems," *IEEE J. Select. Areas Commun.*, vol. 10, pp. 328–343, Feb. 1992.
[32] G. Caire, R. De Gaudenzi, G. Gallinaro, R. Lyons, M. Luglio, M. Ruggieri, A. Vernucci, and H. Widmer, "ESA satellite wideband CDMA radio transmission technology for the IMT-2000/UMTS satellite component: Features & performance," presented at the IEEE GLOBECOM'99, Rio de Janeiro, Brazil, Dec. 5–9, 1999.
[33] ——, "Development and validation of a wideband CDMA IMT-2000 physical layer for satellite applications," in *Proc. IMSC'99*, Ottawa, ON, Canada, June 1999.
[34] F. Adachi, M. Sawahashi, and H. Suda, "Wideband DS-CDMA for next-generation mobile communications," *Commun. Mag.*, pp. 56–69, Sept. 1998.
[35] F. D. Natali, "AFC tracking algorithms," *IEEE Trans. Commun.*, vol. COM-32, Aug. 1984.
[36] Satellite UMTS Family Radio Access Network Specifications Issue 1 (2000, Oct.). [Online]. Available: http://www.etsi.org

Daniel Boudreau received the B.Eng. degree from the University of Sherbrooke, Sherbrooke, Québec, Canada, in 1982, the M.Eng. degree from Carleton University, Ottawa, ON, Canada, in 1987, and the Ph.D. degree from McGill University, Montréal, Québec, in 1990, all in electrical engineering.

From 1983 to 1987, he was with the Communications Processing Group of the Communications Research Centre (CRC), Ottawa, ON, where he was involved in the design of the first generation of modems for the Canadian Mobile Satellite program. From 1987 to 1990, he was on educational leave from CRC while pursuing the Ph.D. degree in the fields of delay estimation and adaptive filtering. From 1990 to 2000, he conducted research and development in the area of narrow-band modulation techniques, adaptive equalization, and joint source and channel coding for mobile fading channels. He was also actively involved in the R&D of signal processing for spectrum monitoring and automatic modulation recognition. Since September 2001, he has been with the Wireless Technology Laboratories of Nortel Networks, Ottawa, managing projects in the area of signal-processing R&D for the evolution of third-generation cellular systems.

Giuseppe Caire (S'91–M'94) was born in Torino, Italy, on May 21, 1965. He received the B.Sc. degree in electircal engineering from Politecnico di Torino, Italy, in 1990, the M.Sc. degree in electrical engineering from Princeton University, Princeton, NJ, in 1992, and the Ph.D. degree from Politecnico di Torino in 1994.

He is an Associate Professor with the Department of Mobile Communications, Institute Eurecom, Sophia-Antipolis, France. He was with the European Space Agency, ESTEC, Noordwijk, The Netherlands, in 1995. He visited the Institute Eurecom, Sophia Antipolis, France, in 1996 and Princeton University in summer 1997. He was Assistant Professor in Telecommunications at the Politecnico di Torino from 1994 to 1998. He is coauthor of more than 30 papers in international journals and more than 60 papers in international conferences. He is the author of three international patents with the European Space Agency. His interests are focused on digital communications theory, information theory, coding theory, and multiuser detection, with particular focus on wireless terrestrial and satellite applications.

Prof. Caire received an AEI G. Someda Scholarship in 1991, a COTRAO Scholarship in 1996, and a CNR Scholarship in 1997. He was Associate Editor for CDMA and Multiuser Detection of the IEEE TRANSACTIONS ON COMMUNICATIONS from 1998 to 2001. He is currently Associate Editor for Communication Theory of the IEEE TRANSACTIONS ON INFORMATION THEORY.

Giovanni Emanuele Corazza (M'92) was born in Trieste, Italy, in 1964. He received the Dr. Ing. degree *(cum laude)* in electronic engineering from the University of Bologna, Italy, in 1988 and the Ph.D. degree from the University of Rome "Tor Vergata," Italy, in 1995.

From 1989 to 1990, he was with the Canadian aerospace company COM DEV, Cambridge, ON, where he worked on the development of microwave and millimeter-wave components and subsystems. From 1991 to 1998, he was with the Department of Electronic Engineering, University of Rome "Tor Vergata," as a Research Associate. In November 1998, he joined the Department of Electronics, Computer Science, and Systems (DEIS), University of Bologna, where he is presently an Associate Professor and Chair for telecommunications. He leads the group from the University of Bologna participating in the European Community fifth framework project SATIN. During 1995, he visited ESA/ESTEC, Noordwijk. The Netherlands, as a Research Fellow, During 1996, he was a Visiting Scientist with the Communications Sciences Institute, University of Southern California, Los Angeles. The same institute invited him to teach a course on Spread Spectrum Systems in fall 2000 as a Visiting Professor. During summer 1999, he was a Principal Engineer at Qualcomm, San Diego, CA. His research interests are in the areas of communication theory, wireless communications systems, spread-spectrum techniques, and synchronization.

Prof. Corazza is an Associate Editor for Spread Spectrum for the IEEE TRANSACTIONS ON COMMUNICATIONS. He received the Marconi International Fellowship Young Scientist Award in 1995 *(ex aequo)*. He was corecipient of the Best Paper Award at the IEEE Fifth International Symposium on Spread Spectrum Techniques & Applications (ISSSTA'98), September 1998, Sun City, South Africa.

Riccardo De Gaudenzi (M'88–SM'97) was born in Italy in 1960. He received the Dr. Eng. degree in electronic engineering *(cum laude)* from the University of Pisa, Italy, in 1985 and the Ph.D. degree from the Technical University of Delft, The Netherlands, in 1999.

From 1986 to 1988, he was with the Stations and Communications Engineering Department, European Space Agency (ESA), Darmstadt, Germany, where he was involved in satellite telecommunication ground systems design and testing. In particular, he followed the development of two new ESA satellite tracking systems. In 1988, he joined ESA's Research and Technology Centre (ESTEC), Noordwijk, The Netherlands where is presently Head of the Communication Systems Section. He is responsible for the definition and development of advanced satellite communication systems for fixed and mobile applications. He is also involved in the definition of the Galileo European satellite navigation system. He spent 1996 with Qualcomm Inc., San Diego, CA, in the Globalstar LEO project system group under an ESA fellowship. His current interest is mainly related to efficient digital modulation and access techniques for fixed and mobile satellite services, synchronization topics, adaptive interference mitigation techniques, and communication system simulation techniques.

Dr. De Gaudenzi is currently an Associate Editor for CDMA and Synchronization for IEEE TRANSACTIONS ON COMMUNICATIONS.

Gennaro Gallinaro received the Dr.Ing. degree in electronic engineering *(cum laude)* from the University of Rome, Italy, in 1979.

From 1981 to 1989, he worked in Telespazio, Rome, where he was involved in satellite telecommunication system planning and design. Since 1989, he has been with Space Engineering, Rome. His main interests are presently in digital transmission system analysis and simulation, mobile communication, and digital signal processing.

Michele Luglio received the Laurea degree in electronic engineering and the Ph.D. degree in telecommunications from University of Rome "Tor Vergata," Italy, in 1990 and 1994, respectively.

His thesis regarded the Public Switched Telephone Network (PSTN), which has been awarded by Consorzio Roma Ricerche (CRR). From August to December 1992, he was a Visiting Staff Engineer at the Microwave Technology and Systems Division, Comsat Laboratories, Clarksburg, MD. Since October 1995, he has been a Research and Teaching Assistant at University of Rome "Tor Vergata," where he works on designing satellite systems for multimedia services both mobile and fixed in the frame of projects funded by EC and ESA. He taught signal theory and collaborated in teaching digital signal processing and elements of telecommunications. During winter 2001, he taught a satellite networks class at the University of California Los Angeles Computer Science Department. He now teaches deterministic signals and satellite telecommunications.

Dr. Luglio received the Young Scientist Award at ISSSE'95.

R. Lyons received the B.Sc. degree in engineering and mathematics and the M.Sc. degree in mathematics from Queen's University, Canada, in 1967 and 1968, respectively, and the Ph.D. degree in electrical engineering from Carleton University, Canada, in 1971.

He has many years of technical and managerial experience in the development of analog and digital communications systems and products. He is a Cofounder and President of both Square Peg Communications Inc. and Terrapin Communications Inc. in Ottawa. He was previously Vice-President and General Manager of Calian Communications Systems Ltd. (1993–1995) and President, SkyWave Electronics Ltd. (1984–1993). Before that, he was with Miller Communications Systems, Ltd., Telesat Canada, and BNR.

Javier Romero-García was born in Málaga, Spain, in 1971. He received the M.S. degree in telecommunication engineering from the University of Málaga in 1995. He is pursuing the Ph.D. degree with the Communication Engineering Group, University of Málaga.

From 1995 to 1997, he was an Associate Professor at the University of Málaga. During 1997 and 1999, he was researching at the European Space Research and Technology Centre, The Netherlands. Since 1999, he has been with Nokia Networks. His main research interests are CDMA interference cancellation and performance of CDMA and TDMA communication systems.

A. Vernucci graduated in electronic engineering from the University of Rome, Italy, in 1972.

He has been Telecommunications Program Director at Space Engineering, Rome, since 1989. Eventually, he joined Telespazio, Rome, where he was involved in several research projects concerning satellite digital data transmission and on-the-air trials. He participated in several standardization groups within CEPT, Intelsat, and Eutelsat. He was Project Manager for Italsat, the Italian Ka-band SS-TDMA system launched in 1990. He was deeply involved in several ESA activities, noticeably the OBP project. More recently, he has been dealing with mobile satellite projects, mainly ESA- or EC-funded, with particular regard to CDMA transmission issues. His main interests are system architectures, access techniques, network integration, and on-board processing. He is the author of numerous papers submitted to major communication conferences (AIAA, GLOBECOM, ICC, ISS, IMSC, etc.).

Hanspeter Widmer was born in Schaffhausen, Switzerland, on December 2, 1955. He received the M.Sc. and Ph.D. degrees in electrical engineering from the Federal Institute of Technology (ETH), Zurich, Switzerland, in 1979 and 1991, respectively.

In 1980, he was with the Telecom Service, International Committee of the Red Cross, in charge of operation and maintenance of HF and VHF radio networks in Africa and Far East. From 1981 to 1988, he was an Assistant with the Microwave Laboratory of the ETH, teaching in fundamental electrical engineering, transmission-line theory, and microwave techniques. In 1984, he started new research activities in the area of extremely robust and energy-efficient communication techniques. He joined the Ascom group in 1988 as a Research Engineer. He was working in the fields of military HF radio communications, private mobile radio, and wireless LAN. Currently, his research activities are mainly concerned with UMTS, mobile satellite, and power-line communications.